THE GEOLOGICAL SOCIETY OF AMERICA

Cenozoic alkaline volcanism of the Atakor massif, Hoggar, Algeria

Abla Azzouni-Sekkal*
*Faculté des Sciences de la Terre, de l'Aménagement du Territoire et de la Géographie, Université des
Sciences et Techniques Houari Boumediene, B.P. 32, El Alia, 16111 Bab Ezzouar, Algiers, Algeria*

Bernard Bonin*
UMR 8148 "IDES," Département des Sciences de la Terre, Université de Paris-Sud, F-91405 Orsay Cedex, France

Amel Benhallou*
Centre de Recherches en Astronomie, Astrophysique, et Géophysique, Bouzaréah, Algeria

Rachid Yahiaoui
École Normale Supérieure, Kouba, Algiers, Algeria

Jean-Paul Liégeois*
Isotope Geology, Musée Royal de l'Afrique Centrale, B-3080 Tervuren, Belgium

ABSTRACT

The Atakor massif is a part of the Hoggar volcanic province, which was emplaced on top of a basement swell initiated during the Cretaceous. There have been three main episodes of volcanic activity since the Miocene, separated by long periods of quiescence. The lava flows and domes were emitted along lithosphere-scale fault zones. With its famous scenery, the Atakor massif is one of the largest (2150 km²) volcanic districts of the province. Mafic volcanic rocks are abundant in the center of the massif, but become scarce to the south, where only few scarps are observed. Phonolites occur only in the Assekrem area, whereas trachytes occur everywhere, with a marked enrichment in quartz to the south and the southeast (Tahifet area), where rhyolites are also exposed. Two magmatic groups have been identified based on field and petrological observations. The mafic group has a basanite-phonotephrite association, forming uplifted plateaus, scoria cones, and valley-filling lava flows. The presence of mantle-derived amphibole ± biotite megacrysts and peridotite mantle xenoliths together with the nonprimary chemical compositions of the magmatic rocks suggest that magmatic differentiation may have occurred within the upper mantle. The felsic group is composed of two diverging trends, a silica-saturated benmoreite-trachyte-rhyolite trend and a silica-undersaturated trachyte-phonolite trend. The primary magmas are considered to have been produced as a consequence of lithospheric mantle delamination along linear megashear zones inducing low degrees of decompression partial melting at variable depths (110–40 km) in the upwelling asthenosphere. The discrete volcanic episodes correspond to periods of reactivation of the major fault zones in response to discrete Neogene extensional tectonic events associated with Alpine orogenesis in the Western Mediterranean region induced by Africa-Eurasia collision.

Keywords: Hoggar (Algeria), volcanism, alkali basalt, phonolite-trachyte, upper mantle.

INTRODUCTION

The Mediterranean Sea is the product of a complex series of plate tectonic processes. It corresponds broadly to an extensional tectonic system overlying the convergence zone between the European continental plate to the north and the African continental plate and related microplates to the south (e.g., Jolivet and Faccenna, 2000; Rosenbaum et al., 2002; Frizon de Lamotte, 2006). Oceanic domains emplaced in between continental blocks are exposed as small ophiolite slices, or have been consumed through subduction beneath the Italian peninsula and the Aegean Sea, as well as along the Rif-Tell belts in North Africa. The present-day tectonic settings include both continent-continent collisional and postcollisional regimes (Jolivet et al., 1999). Numerous magmatic provinces developed along seismically active tectonic lineaments within the Alps and Apennine fold belts (Lustrino, 2000; Savelli, 2002 and references therein), as well as further inland within the adjacent continents of Africa (Black and Girod, 1970) and Europe (Wilson and Downes, 1991).

The Cenozoic volcanic province of Hoggar (also named Ahaggar in the literature) is located within the African plate ~1200 km south of the Mediterranean coast (Fig. 1). It is composed of several massifs of contrasting ages and eruptive styles, covering a total area of ~11,700 km^2, with an eruptive volume of ~1650–2500 km^3. The volcanic formations rest upon uplifted, weathered, and eroded Archean to Neoproterozoic basement. Magmatic activity began at the Eocene-Oligocene boundary ca. 34 Ma (Aït Hamou et al., 2000) and has continued until the present (Girod, 1971). Associated with a crustal swell, 1000 km in long axis, the Hoggar volcanic province is classically considered to be the product of a mantle plume (Sleep, 1990; Burke, 1996), although no significant thermal anomaly has been detected, nor is uplift limited to the central Hoggar area. Clear links are evident between Cenozoic volcanism in West Africa and Pan-African tectonic lineaments, and also between the timing of volcanism and Alpine orogenic events (for a review and discussion, see Liégeois et al., 2005).

The Atakor massif is located right in the center of the Hoggar swell (Fig. 2). Its volcanic formations cover an area of 2150 km^2 with a total volume estimated at ~250 km^3; this corresponds to ~10%–15% of the entire Hoggar volcanic province. Because of its exceptional position within the swell and the excellent exposure, most attention has been focused on the Atakor massif (e.g., Allègre et al., 1981). New whole-rock major-, trace-element, and mineral chemical data are presented here that allow us to reconstruct the evolution in space and time of the Atakor Neogene volcanic episodes and their geodynamic relationships with the evolving Alpine orogenic system.

Sampling and Analytical Techniques

Three districts of the Atakor massif were investigated in this study. The Tahifet area in the southeast (Benhallou, 2000) had never been studied before. The Assekrem plateau and nearby formations in the central part of the massif (Yahiaoui, 2003) and the volcanic edifices near Tamanrasset in the southwest were previously studied by Girod (1971). Representative samples, collected on the basis of apparent lack of alteration in the field were analyzed for their bulk-rock and mineral chemistry. Bulk-rock sample powders were prepared at Centre de Recherches Pétrographiques et Géochimiques (CRPG), Nancy (France), followed by fusion with LiBO$_2$ and HNO$_3$ dissolution, and analysis by inductively coupled plasma–electron spectrometry (ICP-ES; major and minor elements) and inductively coupled plasma–mass spectrometry (ICP-MS; trace elements, with analytical uncertainties ranging from 5% to 20%, according to the element and the concentration), with quality control using international geostandards. Representative whole-rock compositions are listed in Tables 1 and 2. Minerals were analyzed using the CAMEBAX electron microprobe at the Université de Paris–Sud, Orsay, using routine techniques, i.e., natural minerals as standards, 15 kV acceleration voltage, 12 nA beam intensity, and 10 s counting times.

GEOLOGICAL SETTING OF THE MAGMATISM

The volcanic formations of the Atakor massif are exposed at high altitudes, often more than 2000 m above sea level (asl). The highest peak is the 2918-m-high Tahat phonolite dome. The basement constitutes a large SW-NE–trending dome structure, has altitudes consistently above 1400 m asl, and culminates in a small, 2570-m-high, Precambrian basement inlier exposed south of Assekrem and a 2710-m-high phonolite lava dome (Girod, 1971). Contrasting morphologies, which result from recent tectonic uplift, erosion of the basement, and contrasting eruptive styles, dominate the landscape (Fig. 3). Outpouring of mafic magmas produced extensive lava flows that form large, dissected plateaus, or have filled valleys associated with scoria cones and necks. More viscous, felsic magmas were extruded as domes and spines associated with and intruding pyroclastic deposits and rare thick lava flows. Detailed field descriptions can be found in Rognon (1967) and Girod (1971).

Age of Magmatism

Radiometric dates for the magmatic rocks of the Atakor massif are scarce. Coupled with sedimentological constraints, such as the presence of lacustrine travertine and diatomite, geomorphological observations, such as alluvial terraces (Rognon, 1967), and paleontological data, such as silicified wood (Rognon et al., 1983), available K/Ar isotopic and ^{14}C data indicate three discrete episodes of eruptions, separated by two periods of quiescence:

1. The first, and the most voluminous, magmatic episode occurred during the Miocene from 19.9 ± 1.9 Ma to 12.4 ± 2 Ma, i.e., from the Burdigalian to the Serravallian (according to the most recent geological time scale, Gradstein et al., 2004). Flood basalts, intercalated with trachytic tuffs (redefined as benmoreite, see following), form a large plateau. The episode ended with the emplacement of the 2918-m-high Tahat phonolite dome. Other

1000 km

Az= Azrou
Ta= Taourirt
GB= Grande Kabylie
KH= Kef Hahouner
H-A= High Atlas
M-A= Middle Atlas
S-A= Saharan Atlas
A-A= Anti-Atlas
Tam=Tamanrasset

France

Spain

Italy

Penadriatic line

Morocco

Rabat

Rif

Oran

Alger KB

Oranie

Tell

KH Nefza

Tunis Tunisia

Az M-A Ta

Oulmès

Rekkame

S-A

36

Tripoli

Tamazert

Laghouat

H-A

Sirwa

A-A

Sahro

Gharyan

N

Algeria

Libya

30°

West

African

craton

Hoggar

Egéré

Al Hasawinah

As Sawda

?

Murzuq

In Teria

n'Ajjer

Al

Haruj

Taoudeni

Manzaz

Atakor

Anahef

Djanet

Tam

Tahalra

In Ezzane

Djado

Mali

Tin

Zaouatene

Aïr

20°

Tibesti

Timbuctu

Gao

Iforas

Todra

Agadès

Tin Taralle

Niger

10°

Chad

0°

	Phanerozoic sedimentary cover		Archean, Paleoproterozoic and Neoproterozoic terranes affected by the Pan-African orogeny
	Cenozoic volcanism		Archean and Paleoproterozoic West African craton and its sedimentary cover
	Atlas mountains		

Major Pan-African shear zones

Inferred major Pan-African shear zones

Uplifts structures in Libya

Mediterranean shear zones

Thrusts

Figure 1. Cenozoic volcanism in NW Africa and the Western Mediterranean. Map is based on Fabre (2005); Black et al. (1967, 1994); Saadi (1982); Savelli (2002); Vai (2001); Bigi et al. (1989). The volcanic fields in the Tuareg shield were drawn from a satellite photograph; orthorectified Landsat Thematic Mapper mosaics as compressed color imagery in MrSIDTM file format are from Lizardtech.
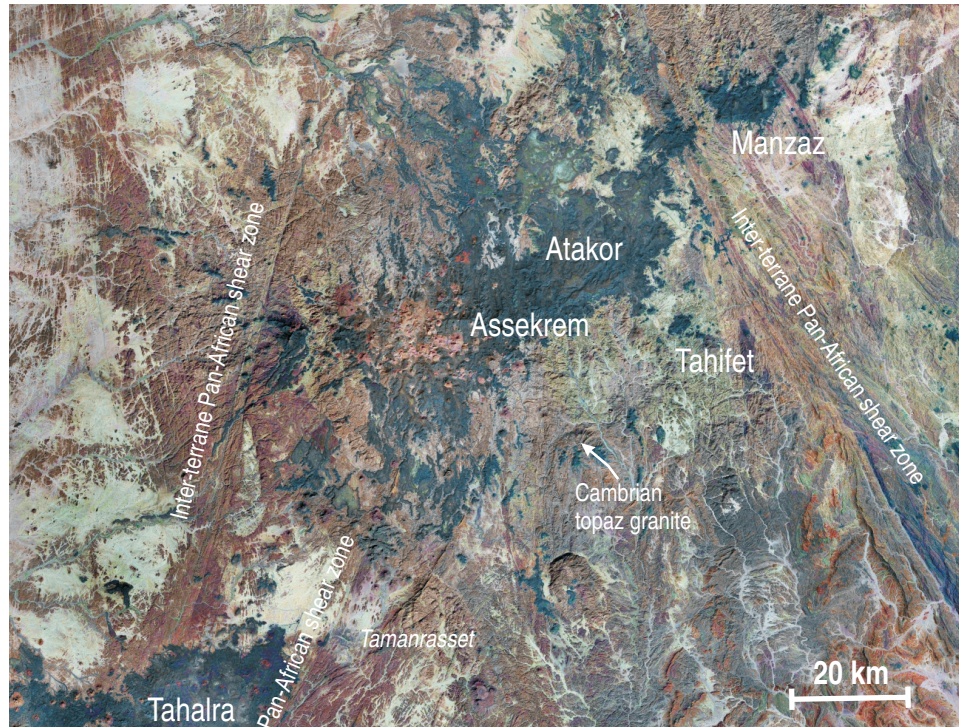
Figure 2. Satellite photograph of the Atakor massif (orthorectified Landsat Thematic Mapper mosaics as compressed color imagery in MrSIDTM file are from Lizardtech). The Atakor massif is located in between the Manzaz district to the northeast, and the Tahalra district to the southwest. The lavas appear dark blue and the scoria cones red or brown due to several factors, including iron oxidation. The linear eastern boundary corresponds to a Pan-African shear zone within the LATEA metacraton.

high-altitude domes and flows emplaced onto the basaltic plateau, such as the undated Assekrem phonolite dome and related Zermezoug lava flow, could belong to the same stage. Morphological observations (Girod, 1971) suggest that the igneous episode was not coeval with any large tectonic displacements.

A long period of quiescence of ~6 m.y. took place between 12.4 ± 2 Ma and 6.7 ± 2 Ma, i.e., during the Tortonian. The older scoria cones were eroded, and their remnants, such as the basaltic tuffs and ash deposits that are exposed under the Akarakar trachyte complex, are preserved under the deposits of the subsequent magmatic episodes. The more resistant lava plateau was dissected by water-driven erosion.

2. The second magmatic episode began after the Tortonian period of quiescence. It spanned the Miocene-Pliocene boundary from 6.7 ± 2 Ma to 4.2 ± 0.2 Ma, i.e., from the Messinian to the Zanclean. The erupted products are compositionally more variable, ranging from basalt to phonolite (Girod, 1971; Rognon et al., 1983). Available data suggest that the episode started with the emplacement of phonolite and trachyte domes, spines, and flows, and ended with the outpouring in western Atakor of mafic plateau-forming lava flows.

An ~2.25 m.y. period of magmatic quiescence, from 4.2 ± 0.2 Ma to 1.95 ± 0.2 Ma, i.e., during most of the Pliocene, was marked by active normal faulting and complete resurfacing of

the massif. The older scoria cones were again destroyed by erosion and can be clearly distinguished from the morphologically younger scoria cones of the most recent volcanic episode. The original topography was inverted, so that the plateau-forming and older valley-filling basaltic lava flows are now exposed as dissected cliffs and scarps. The felsic domes, spines, and flows occur on top of hills composed of Precambrian basement capped by a thick blanket of pyroclastic deposits. On the basis of the variations in basement altitudes from 1390 m in the city of Tamanrasset to 2570 m in the Assekrem inlier, the total amount of uplift is estimated at ~1200 m, which corresponds to an average crustal uplift rate of 0.5 ± 0.1 mm yr^{-1} during a period of 2.25 m.y.

3. The final magmatic episode started after the Pliocene period of quiescence, from 1.95 ± 0.2 Ma to the present, i.e., from the Gelasian to the Holocene. The erupted products are exclusively basanites-tephrites that form scoria cones, necks, and valley-filling lava flows, which constitute less than 3% of the total area of the Atakor massif (Rognon et al., 1981, 1983). Some lava flows, emitted from the freshest-looking scoria cones, cover Holocene lacustrine formations, dated by ^{14}C at ca. 10 k.y. B.P. (cited by Girod, 1971). To the north, small basanite lava flows cover the youngest alluvial terrace, in which Neolithic artifacts have been found in situ (Rognon, 1967). Moreover, the Tuareg people relate ancestral stories suggesting that the volcanoes were

TABLE 1. REPRESENTATIVE WHOLE-ROCK (MAJOR AND TRACE ELEMENTS) COMPOSITIONS OF MAFIC ROCKS

Sample number:	IA8	IJ1	IJ2	SA06	ISK7	SA03	PAS06	TAH01	BS01	Y6A
SiO_2	42.73	43.24	43.93	44.05	45.25	50.44	43.64	49.66	46.77	46.88
TiO_2	3.76	3.79	3.64	3.49	3.14	2.04	3.29	2.25	2.23	3.02
Al_2O_3	14.12	14.44	15.17	15.95	15.34	17.96	15.37	16.62	16.17	14.71
$Fe_2O_3^{t}$ *	14.44	14.41	14.44	13.77	12.86	9.25	13.54	10.28	10.67	11.95
MnO	0.18	0.19	0.19	0.20	0.17	0.25	0.19	0.18	0.20	0.18
MgO	7.57	7.03	6.19	5.79	5.66	2.67	7.39	4.93	5.65	7.73
CaO	10.06	9.57	9.07	9.20	9.48	6.52	10.86	6.88	9.38	8.79
Na_2O	2.79	3.55	3.54	3.68	3.17	5.99	3.34	4.22	5.04	4.52
K_2O	1.54	1.40	1.90	1.08	1.57	3.11	1.47	2.98	1.96	1.64
P_2O_5	0.87	0.93	1.12	0.70	0.81	0.85	0.88	0.65	0.84	0.54
LOI ^{t}	1.94	1.66	0.81	1.69	2.54	1.02	0.49	1.37	1.04	0.39
Total	100.00	100.21	100.00	99.60	99.99	100.10	100.46	100.02	99.95	100.35
Rb §	32.6	38.7	32.8	40.7	29.5	91.34	31.96	66.7	57.15	30.0
Cs	0.19	0.22	0.20	0.25	B.D.L.	1.26	0.363	0.36	0.708	0.64
Be	1.23	1.52	1.22	1.99	1.30	3.57	1.42	2.16	3.18	2.02
Sr	882	832	911	873	821	1302	830	618	1458	973
Ba	425	451	440	597	401	1085	506	737	960	663
Y	31.6	32.4	33.2	28.5	29.0	50.7	27.8	22.6	36.0	27.2
La	52.2	54.7	56.1	51.6	52.6	154.5	47.25	57.6	114.7	65.0
Ce	108	118	123	107	110	296.5	96.38	108	204.1	135
Pr	13.2	14.0	14.7	13.2	12.4	32.77	11.24	11.2	22.29	14.9
Nd	56.0	59.1	60.9	51.9	49.6	116.3	45.78	42.2	76.46	57.1
Sm	10.8	11.8	12.2	10.4	9.89	17.94	8.81	7.73	13.07	10.1
Eu	3.51	3.56	3.65	3.17	3.09	5.15	2.6	2.49	3.62	3.32
Gd	9.14	9.34	9.50	8.31	7.75	14.04	6.91	5.89	10.41	8.26
Tb	1.24	1.28	1.33	1.11	1.06	1.88	1.02	0.827	1.36	1.09
Dy	6.27	6.68	6.89	6.17	5.74	10.12	5.46	4.22	6.58	5.82
Ho	1.17	1.24	1.22	1.14	1.03	1.68	0.91	0.795	1.11	1.10
Er	2.73	2.90	2.87	2.57	2.49	4.91	2.34	2.10	2.85	2.42
Tm	0.324	0.333	0.373	0.339	0.363	0.66	0.3	0.267	0.35	0.304
Yb	2.15	2.34	2.28	2.28	2.15	3.67	1.91	1.83	2.32	1.93
Lu	0.308	0.303	0.320	0.312	0.265	0.59	0.236	0.265	0.31	0.273
Th	5.80	6.20	6.15	6.91	5.82	19.38	6.75	9.36	15.33	7.65
U	1.44	1.65	1.7	1.48	1.60	3.84	1.58	2.48	4.0	2.06
Zr	289	308	324	273	310	591	262	336	453	412
Hf	6.72	7.07	7.02	6.24	6.33	10.8	5.62	6.58	8.19	8.68
V	273	263	222	267	191	121	297	137	213	207
Nb	73.8	77.2	80.0	86.9	72.3	247.2	76.06	86.9	143.8	93.4
Ta	5.47	5.81	5.88	6.31	5.14	21.14	5.22	5.91	10.72	6.49
Cr	217	180	79.8	61.9	121	6.56	102	93.7	215	284
Mo	1.37	2.11	2.70	2.35	2.31	6.45	2.81	3.94	7.51	4.57
W	0.40	0.50	0.41	0.76	0.71	1.69	0.74	0.79	2.7	0.86
Co	49.2	47.1	40.1	49.2	37.9	17.1	49.7	26.7	32.7	47.1
Ni	106	85.9	54.2	59.1	73.3	4.18	76.1	63.4	80.6	168
Cu	54.5	49.0	40.1	49.7	38.2	14.0	65.4	27.6	31.7	51.5
Zn	154	159	157	148	140	154	145	119	156	143
Cd	0.26	0.21	0.31	0.23	B.D.L.	0.38	0.85	0.36	1.18	0.57
Ga	22.2	24.0	21.5	22.0	21.4	25.4	23.1	21.5	23.8	22.5
In	0.10	B.D.L.	0.10	B.D.L.	B.D.L.	0.08	0.16	B.D.L.	0.17	B.D.L.
Ge	1.03	1.07	1.04	1.11	1.04	1.4	1.32	0.84	1.31	1.02
Sn	1.97	2.31	2.01	2.07	1.79	2.76	2.61	1.79	2.43	1.85
Pb	3.38	3.20	3.04	5.27	3.35	7.76	3.75	5.63	12.4	3.93
As	0.71	0.81	1.06	0.88	0.70	1.81	0.8	1.48	3.12	0.97
Sb	B.D.L. #	B.D.L.	0.10	B.D.L.	B.D.L.	0.25	0.11	B.D.L.	0.32	0.12
Bi	Traces **	Traces	B.D.L.	Traces	Traces	0.04	0.17	Traces	0.19	Traces

* Total iron determined as wt% Fe_2O_3.
^{t} LOI = Loss on Ignition (wt%).
§ Trace elements (in ppm) are arranged in the increasing order of columns of the periodic table of elements and of atomic numbers.
B.D.L. = Below detection limit.
** Traces: No detection
IA8 Miocene basanite lava flow, South Tahifet area.
IJ1 Miocene basanite lava flow, South Tahifet area.
IJ2 Miocene basanite lava flow, South Tahifet area.
SA06 Miocene basanite lava flow, Northwest Assekrem area.
ISK7 Miocene alkali basalt lava flow, Isekram, Tamanrasset area.
SA03 Miocene phonotephrite lava flow, Northwest Assekrem area.
PAS06 Miocene—Pliocene basanite neck, Assekrem plateau.
TAH01 Miocene—Pliocene mugearite neck, Tahaleft, Assekrem area.
BS01 Pliocene tephrite lava flow, Oued Segueïka, Assekrem area.
Y6A Pliocene—Quaternary hawaiite neck, North Tahifet area.

TABLE 2. REPRESENTATIVE WHOLE-ROCK (MAJOR AND TRACE ELEMENTS) COMPOSITIONS OF FELSIC ROCKS

Sample number:	TIL8	TIN3	OTAB01	SKR6	TEZ06	ADRN4	Y1C1	IM2	TEZ01	Y1F1	N1B	LHA6	Y2A4	PAS01	DEB2'
SiO_2	59.52	61.38	61.77	62.34	62.73	62.81	64.73	65.80	66.81	66.82	67.47	67.61	70.59	60.19	59.81
TiO_2	0.71	0.4	0.32	0.26	0.16	0.33	0.32	0.20	0.09	0.27	0.21	0.16	0.11	0.30	0.04
Al_2O_3	18.03	17.42	17.09	17.43	17.94	17.79	17.48	15.53	16.10	16.01	16.32	14.84	15.31	19.59	18.81
$Fe_2O_3^t$	5.68	5.22	5.42	5.17	3.34	4.50	3.55	4.30	2.99	3.61	3.25	4.20	1.05	3.40	5.07
MnO	0.24	0.29	0.27	0.34	0.13	0.67	Traces	0.15	0.12	0.05	0.06	0.28	Traces	0.21	0.23
MgO	1.35	0.81	0.36	0.52	0.22	0.23	Traces	0.17	0.15	0.17	0.08	0.08	0.16	0.24	0.26
CaO	1.39	1.38	1.39	0.80	0.70	0.68	0.45	0.71	0.64	0.75	0.46	0.55	0.35	0.98	1.26
Na_2O	6.09	7.13	7.14	7.00	6.21	7.04	5.99	7.07	6.83	5.43	5.57	6.80	4.91	8.02	8.59
K_2O	4.84	5.01	5.08	5.15	4.74	4.92	5.61	4.75	4.55	5.31	5.31	4.53	4.40	5.57	5.13
P_2O_5	0.38	0.27	0.2	0.16	0.11	0.23	0.12	0.08	0.11	0.11	0.17	0.02	0.05	0.04	0.14
LOI	1.76	0.64	0.91	0.75	3.43	0.73	2.04	0.80	1.17	1.82	1.37	0.89	2.57	1.43	0.60
Total	99.99	99.95	99.95	99.92	99.71	99.93	100.30	99.56	99.56	100.35	100.27	99.97	99.50	99.97	99.94
Rb	113	132.7	172.5	127	353	115	191.2	313.4	269	165.5	204.8	308	345	268	227
Cs	0.47	1.63	1.06	0.54	18.65	0.29	0.916	1.36	0.785	0.443	0.922	0.68	1.24	2.18	1.47
Be	2.90	4.5	7.33	4.53	15.6	4.63	5.97	12.4	3.4	4.73	3.27	12.1	7.57	9.09	9.74
Sr	313	70.7	41.5	31.1	39.6	60.2	23.4	21.7	35.7	16.0	15.3	17.4	36.8	38.0	64.4
Ba	972	311	58	189	41	527	34	30	34	36	25	22.8	13	49.7	21
Y	21.7	38.3	60.3	37.6	62.0	31.7	44.5	91.9	74.9	55.0	46.7	62.1	62.6	34.6	78.9
La	71.6	109.4	163.1	103	142	95.6	95.38	263.5	62.16	112	62.03	120	48.26	156	228.6
Ce	149	195.5	283.6	182	253.3	182	132	440	129.4	221.6	208.1	229	79.71	226	420.4
Pr	13.9	19.78	29.94	17.7	27.07	18.3	18.9	47.8	14.63	22.33	14.16	21.1	8.8	19.0	44.6
Nd	46.4	65.16	95.12	56.7	84.85	60.7	64.23	156.5	48.68	72.28	48.56	62.4	26.75	49.6	148
Sm	7.20	10.68	15.38	9.08	13.71	9.38	10.96	26.49	9.56	12.68	9.03	10.5	6.07	6.61	23.17
Eu	2.52	2.23	1.51	1.57	1.28	1.96	0.59	0.77	0.544	0.61	0.526	0.401	0.08	0.731	0.77
Gd	4.72	7.46	11.31	6.69	10.48	6.85	8.96	20.01	8.12	10.62	7.54	8.64	6.37	5.11	16.86
Tb	0.774	1.17	1.67	1.05	1.7	1.04	1.34	2.96	1.55	1.73	1.34	1.57	1.31	0.827	2.70
Dy	3.91	6.92	10.79	6.05	10.38	5.77	7.86	16.52	10.92	10.24	8.15	9.50	9.38	5.11	15.53
Ho	0.786	1.36	2.01	1.27	1.99	1.11	1.51	2.92	2.27	2.01	1.67	2.02	2.18	1.11	2.75
Er	2.05	3.46	5.7	3.46	5.86	3.04	4.04	8.44	6.93	5.51	4.68	5.71	5.96	3.10	8.02
Tm	0.321	0.58	0.91	0.585	1.02	0.481	0.66	1.22	1.16	0.88	0.75	1.03	1.02	0.534	1.20
Yb	1.97	4.02	5.98	4.17	6.53	3.19	4.33	7.66	7.49	5.64	5.02	7.49	6.82	3.82	7.37
Lu	0.282	0.63	1.04	0.602	1.03	0.503	0.68	1.13	1.16	0.81	0.72	1.01	0.91	0.628	1.20
Th	14.3	18.79	29.47	26.7	86.35	19.3	34.07	48.72	41.64	29.54	33.09	58.1	57.12	51.8	43.11
U	2.96	5.92	5.35	4.43	20.44	4.56	5.09	11.87	11.26	6.42	7.53	10.4	12.56	13.6	9.87
Zr	528	718	1001	893	1217	827	954	986	643	778	657	1173	630	1191	1118
Hf	11.1	16.5	24.4	17.9	37.6	16.4	22.3	29.1	23.0	19.8	16.8	34.0	24.4	24.4	32.1
V	7.5	2.53	0.6	B.D.L.	1.91	B.D.L.	2.17	0.99	0.78	3.64	0.25	Traces	Traces	2.60	Traces
Nb	127	171.5	247.8	193	508	163	204.4	379.1	320.8	184.2	189.6	450	294.5	288	365.2
Ta	9.49	13.22	17.65	14.5	52.04	12.7	13.9	29.3	33.18	14.52	14.93	38.5	31.28	19.4	29.42
Cr	B.D.L.	3.03	3.65	Traces	2.82	Traces	4.01	1.79	1.52	3.01	3.56	Traces	6.57	B.D.L.	1.24
Mo	1.46	7.4	4.78	2.83	3.25	3.32	2.08	13.7	1.01	7.4	12.7	5.86	0.55	22.4	2.88
W	0.65	0.71	1.78	1.40	3.28	2.30	3.22	5.54	4.79	4.66	3.41	3.49	3.96	1.45	2.18
Co	3.12	0.75	0.61	0.75	0.86	0.37	0.59	0.57	2.72	0.44	0.50	B.D.L.	0.25	1.22	0.09
Ni	B.D.L.	0.92	1.43	B.D.L.	4.57	B.D.L.	1.15	0.93	0.83	3.17	0.81	B.D.L.	1.10	B.D.L.	Traces
Cu	5.7	2.6	5.2	B.D.L.	6.4	3.8	4.7	4.9	3.9	5.3	5.30	B.D.L.	1.3	7.2	5.6
Zn	121	143	192	143	211	119	67.8	264	230	92.8	151	238	29.8	142	326
Cd	0.35	0.27	0.71	0.25	0.66	0.39	0.55	0.97	0.47	0.43	0.39	0.87	0.35	0.84	0.35
Ga	22.2	24.5	32.5	24.2	48.8	24.1	32.2	47.3	41.6	34.4	35.1	33.9	38.5	34.3	52.9
In	0.12	0.14	0.2	0.12	0.06	B.D.L.	0.1	0.2	0.09	0.17	0.15	0.13	0.12	B.D.L.	0.25
Ge	1.19	1.29	1.85	1.30	2.33	1.18	1.89	2.1	2.12	1.79	1.76	1.61	1.79	1.30	2.26
Sn	2.59	2.98	4.65	3.12	10.2	2.21	5.65	11.2	11.4	5.71	6.74	8.53	13.7	4.75	9.47
Pb	5.90	9.69	16.4	23.9	29.9	9.01	9.79	24.4	29.7	18.9	19.0	26.8	38.6	21.3	29.7
As	0.48	2.02	2.83	0.76	3.49	0.57	1.66	6.39	0.58	2.82	1.30	2.20	1.51	2.07	1.82
Sb	0.13	0.26	0.3	0.22	1.12	0.17	0.28	0.68	0.76	0.6	0.45	0.38	0.39	0.46	0.33
Bi	Traces	0.02	0.04	Traces	0.21	Traces	0.02	0.1	0.01	0.04	0.04	Traces	0.11	B.D.L.	Traces

Note: Same mode of presentation as in Table 1.
TIL 8 Trachyte neck, Tilaouis, near Tamanrasset.
TIN3 Trachyte dome, Tindi, near Tamanrasset.
OTAB01 Trachyte dome, Oued Tabbezet, Assekrem area.
SKR6 Trachyte plateau, Isekram, near Tamanrasset.
TEZ06 Trachyte dome, Tezouiadje, Assekrem area.
ADRN4 Trachyte dome-lava, Adriane, near Tamanrasset.
Y1C1 Trachyte dome, North Tahifet area.
IM2 Aegirine trachyte neck, Imross, South Tahifet area.
TEZ01 Trachyte dome, Tezouiadje, Assekrem area.
YIF1 Trachyte dome, North Tahifet area.
N1B Trachyte neck, Northeast Tahifet area.
LHA6 Trachyte neck, Iharen, near Tamanrasset.
Y2A4 Rhyolite dome, North Tahifet area.
PAS01 Miaskitic phonolite dome-lava, Assekrem plateau.
DEB2' Agpaitic phonolite dome-lava, Debnat, near Tamanrasset.

Figure 3. Atakor landscape viewed from north of Tamanrasset showing flood lava plateau in the background, dome lavas and necks, and Proterozoic basement in the foreground.

actually seen erupting. Sporadic fumaroles, observed by Girod in 1961, persistent, yet local, seismic activity of small amplitude (Grandjean, 1962), and fault-controlled mineral springs with mantle-derived gas emissions provide evidence that the Atakor massif should not be considered as extinct.

Classification of the Volcanic Rocks

In the Atakor literature, the volcanic rocks have typically been named according to a simplified "field" classification. "Basalt" is used for any dark-colored lava flow, and includes both basanite and tephrite, whereas "hawaiite" and "mugearite" correspond to gray lava flows and domes, and include phonotephrites. Likewise, "phonolite" is used for any felsic rocks bearing feldspathoid(s). Its correct use, however, should be restricted to felsic rocks with either more than 10% modal foid in the alkali feldspar-plagioclase-feldspathoid (APF) diagram (Le Maitre, 1989), or located above the silica undersaturated-saturated (U-S) boundary in the total alkalis versus silica (TAS) variation diagram, i.e., having more than 10% normative foid (Le Bas et al., 1986, 1992). According to recommendations of the Subcommission on the Systematics of Igneous Rocks of the International Union of Geological Sciences (IUGS) (Le Maitre, 2002), most "phonolites" of the Atakor massif are not sufficiently silica-undersaturated, and actually plot in the trachyte field.

Based on field evidence, two groups of magmatic rocks, one mafic and one felsic, separated by a "Daly gap" from 51 to 57 wt% SiO_2, have been identified (Tables 1 and 2):

1. The mafic group (83% of the total area) is composed of dark lava flows and scoria cones, which are made up of basalt and basanite, and of gray lava flows, which were previously determined (Girod, 1971) to be hawaiite and mugearite, but which include more strongly silica-undersaturated types, such as phonotephrite (Table 1). Whatever their age of eruption, they constitute a coherent group in the TAS diagram straddling the U-S boundary from basanite-basalt to mugearite-phonotephrite (Fig. 4).

2. The felsic group (17% of the total area) includes pyroclastic formations, lava flows, and the impressive domes, necks, and spines that dominate the landscape. It is composed of benmoreites, miaskitic and agpaitic phonolites, metaluminous and peralkaline trachytes to quartz trachytes, and peraluminous rhyolites (Table 2). Two diverging evolutionary trends that originate in a common ensemble of intermediate rocks (benmoreite and metaluminous trachyte) can be traced in the TAS diagram (Fig. 4): the first trend, from trachyte to phonolite, is characterized by intermediate silica and increasing alkali contents, while the second trend, from trachyte to rhyolite, is marked by increasing silica contents.

The distribution of the various rock types is not random. Mafic rocks are abundant in the center, north, and west of the massif, where they constitute large plateaus, but are scarce in the south, where they occur as scattered outcrops preserved by erosion, and as valley-filling lava flows. Benmoreites, previously classified as trachytes by Girod (1971), occur as tuffs intercalated within the Miocene basalt plateau and also as domes. Phonolites, in the IUGS sense, are widespread in the Assekrem plateau (Yahiaoui, 2003) and Debnat complex, east of Tamanrasset, but notably lacking in the Tahifet area. Trachyte, in the IUGS sense, i.e., including "phonolite" that contains less than 8 wt% CIPW-normative nepheline, occurs everywhere as domes and spines, with related lava flows. A single occurrence of peraluminous rhyolite was discovered in the Tahifet area (Benhallou, 2000).

MAFIC GROUP OF ROCKS

The mafic group is characterized by CIPW nepheline-normative compositions. Although it can be subdivided into compositionally dispersed subtypes, i.e., basanite, basalt, hawaiite, mugearite, and phonotephrite, the range of compositions plots within a rather small area of the TAS diagram (Fig. 4). The ultrabasic to basic (43–47 wt% SiO_2) magmatic rocks have phenocrysts of olivine + clinopyroxene ± plagioclase. The more differ-

Atakor volcanic massif
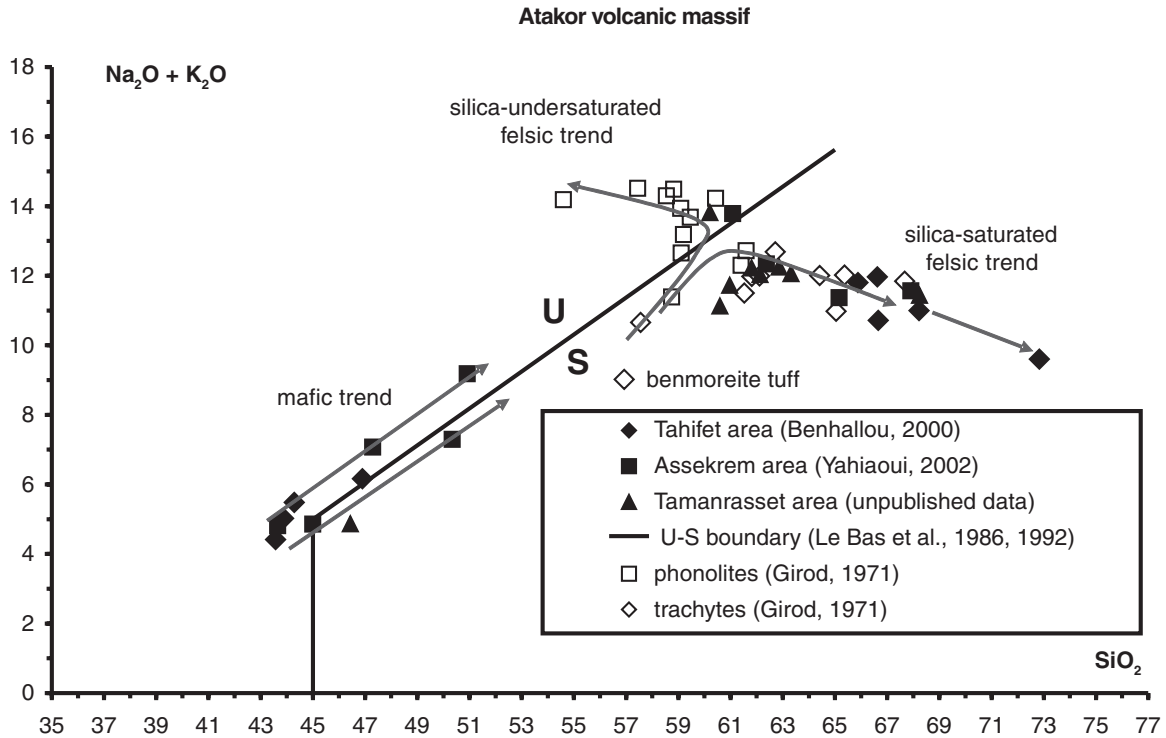
Figure 4. Selected volcanic rock compositions, recalculated on a H_2O- and CO_2-free basis, plotted in the total alkali–silica (TAS) diagram (Le Bas et al., 1986, 1992). The U-S boundary is indicated. Diamonds: Tahifet samples (Benhallou, 2000); squares: Assekrem samples (Yahiaoui, 2003); triangles: Tamanrasset samples (this paper); open symbols: selected samples of benmoreite, phonolite, and trachyte from Girod (1971).

entiated mafic rocks (47–51 wt% SiO_2) have a similar phenocryst mineralogy but with more abundant plagioclase. Widespread secondary "sunburn" analcime occurs in the groundmass.

Mineral Chemistry

Olivine occurs as phenocrysts and microcrysts and contains inclusions of Cr-spinel and Fe-Ti oxides. Iddingsitized rims provide evidence of incipient alteration before and during lava flow eruption. The phenocrysts are normally zoned from $Fo_{87–72}$ cores to $Fo_{74–50}$ rims; the microcrysts have the same compositions as the phenocryst rims. Concentrations of Mn (up to 3.6 wt% MnO) and Ca (up to 0.51 wt% CaO) correlate positively with Fe content.

Clinopyroxene is highly calcic, varying from Al-Ti diopside to diopside to hedenbergite, with phenocryst cores containing more Al and Ti than rims and microcrysts in the groundmass.

Plagioclase is normally zoned from bytownite to labradorite to andesine (An_{71} to An_{39}) in the ultrabasic to basic rocks, and from labradorite to oligoclase (An_{69} to An_{17}) in the more differentiated mafic rocks, in which it coexists with anorthoclase microcrysts.

In addition to the olivine + clinopyroxene + plagioclase microcryst assemblage, the groundmass contains interstitial to poikilitic crystals of analcime and Ti-rich (4.9–8.5 wt% TiO_2) biotite (Girod, 1971; Benhallou, 2000), indicating that fluids were available in fairly large amounts at temperatures close to the solidus. Discrete grains of

ulvöspinel-magnetite and ilmenite-hematite solid solutions, scarce sulfides, such as chalcopyrite and pyrite, abundant apatite, and late-stage carbonates complete the accessory mineral assemblage.

Megacrysts

Megacrysts of Al-Ti diopside and kaersutite, associated with euhedral crystals of zircon and oxide minerals, including Mg-rich ilmenite, occur together with peridotite xenoliths and amphibole-rich enclaves (Dautria et al., 1987). The enclaves have Ti-rich, Si-poor chemistries, and are genetically unrelated to their host rocks, implying that they crystallized under upper-mantle conditions during earlier, undated, igneous episodes. The presence of kaersutite suggests that metasomatic fluids may have modified the subcontinental lithospheric mantle. Based on the occurrence of Mg-rich ilmenite (with 31%–37% geikielite and 10%–25% hematite components) and the abundances of incompatible trace elements in the peridotite xenoliths, Dautria et al. (1988) identified the metasomatizing agent as a kimberlite magma that interacted in small and variable amounts with upper-mantle peridotite.

Kaersutite occurs as unaltered, centimeter-size, euhedral megacrysts in volcanic ash and scoria deposits. It has been partially to totally converted into a plagioclase + clinopyroxene + rhönite + oxides ± olivine assemblage in the basanite-tephrite lava

Figure 5. Kaersutite phenocryst in Miocene mugearite of the Tahaleft neck (photograph from Yahiaoui, 2003). The size of the crystal is ~0.5 mm.

flows (Girod, 1971), whereas fresh phenocrysts (Fig. 5) occur in the mugearite of the Tahaleft neck (Yahiaoui, 2003). Megacrysts of kaersutite are also found in other districts of the Hoggar volcanic province, e.g., Tahalra (Dautria et al. 1987), Manzaz, Adrar N'Ajjer, and Djanet (authors' observations).

An altered megacryst of Ti-rich biotite was observed in a basanite sample from the Tahifet area (Benhallou, 2000). The rim of the megacryst is crowded with exsolved rutile needles, and the core is completely converted into an alkali feldspar + clinopyroxene + rhönite + olivine + ilmenite assemblage.

In addition to mafic silicate megacrysts, euhedral crystals of zircon and octahedral crystals of oxide minerals are found in the scoria deposits. Crystals of spinel-hercynite solid solution are homogeneous and include early Mg-rich ilmenite, or exsolved hematite lamellae and corundum grains. Crystals of ulvöspinel-magnetite solid solution are crowded with exsolved ilmenite-hematite and pseudobrookite lamellae. The complex Fe-Ti oxide assemblage appears to have resulted from fluctuating oxygen fugacity (fO_2) at near-liquidus temperatures (Conquéré and Girod, 1968).

FELSIC GROUP OF ROCKS

The less abundant felsic group is compositionally more varied than the mafic group. Two diverging trends, rooted in the benmoreite + trachyte fields, are evident in the TAS diagram (Fig. 4): these evolve either from trachyte to rhyolite, or from trachyte to phonolite. Both trends contain metaluminous types, which evolve to peralkaline and/or peraluminous end members. In peralkaline types, sodic mafic minerals of the agpaitic sequence crystallized late. Phenocrysts, when present, are chiefly composed of alkali feldspar and calcic mafic minerals.

Common Assemblage of Major Rock-Forming Minerals

Well-aligned alkali feldspar phenocrysts and microcrysts define a trachytic texture. All phenocrysts and most microcrysts are monoclinic (sanidine), and yield a restricted range of compositions from Or_{23} to Or_{45}, consistent with hypersolvus crystallization. Some microcrysts are composed of two discrete populations of sanidine Or_{92-95} and albite Or_{01-10}, and therefore crystallized subsolvus.

In silica-undersaturated felsic rocks, nepheline occurs as euhedral phenocrysts rimmed by analcime. Analcime occurs also as late, poikilitic crystals, rarely accompanied by members of the cancrinite-vishnevite solid solution series. In silica-oversaturated rocks, occasional β-type quartz crystals have euhedral shapes.

The groundmass is speckled with Fe-Ti oxides of the ulvöspinel-magnetite solid solution series that are commonly oxidized to Ti-bearing hematite. The common accessory mineral assemblage includes apatite, zircon, titanite, and rutile.

Rock-Forming Minerals of the Trachyte-Rhyolite Trend

Both peralkaline and peraluminous felsic rock types comprise the trend. The widespread peralkaline suite evolved from metaluminous trachyte to aegirine trachyte. The peraluminous group is composed of biotite-trachyte and rhyolite. A third group, well developed in the Akarakar area (Girod, 1971), is composed of fayalite trachyte, akin to the peralkaline suite.

Fayalite occurs as phenocrysts as well as microcrysts in the groundmass, where it coexists with quartz and/or tridymite. Its optical characteristics indicate it contains less than 10% forsterite (Girod, 1971).

Clinopyroxene is the most abundant mafic mineral in the peralkaline suite. Na-bearing (0.15 Na atoms per formula unit [a.p.f.u.]) hedenbergite is the chief mafic mineral of the Tezouiadje domes. In the Oued Tabezzet dome, phenocrysts are composed of large brown Na-bearing (0.07–0.10 Na a.p.f.u.) hedenbergite cores surrounded by narrow green aegirine augite rims (0.24–0.36 Na a.p.f.u.), whereas green microcrysts in the groundmass are more sodic (0.43 and 0.71 Na a.p.f.u.) aegirine augite. In the Tahifet area, nearly pure (0.89–0.95 Na a.p.f.u.) aegirine occurs as interstitial microcrysts.

Arfvedsonite occurs only as interstitial, poikilitic crystals in the groundmass. Its composition is marked by high K_2O contents (up to 2 wt%), with probable occurrence of Li in the octahedral sites that are not fully occupied by Ti, Al, Fe, Mn, and Mg.

Aenigmatite forms crystals surrounding sanidine and quartz in fayalite trachyte and arfvedsonite trachyte (Girod, 1971). In a Tezouiadje dome (Yahiaoui, 2003), dark-brown crystals of a Ti-bearing (0.21–0.35 Ti a.p.f.u.) mineral surround sanidine crystals in the groundmass. The fairly Ti-poor and Fe-rich composition of this mineral, relative to aenigmatite, suggests that it belongs to the wilkinsonite-aenigmatite (Duggan, 1990) solid solution series. This occurrence of a wilkinsonite-like mineral in a peralkaline trachyte is the third reported so far in the world.

Biotite is rare, occurring only in peraluminous trachytes, as brown-red acicular microcrysts in the groundmass and rarely included within sanidine. Its composition is Ti-rich (~7.00 wt% TiO_2). The absence of detectable halogens (F and Cl) suggests that coexisting fluids were essentially aqueous.

Rock-Forming Minerals of the Trachyte-Phonolite Trend

Metaluminous (miaskitic) and peralkaline (agpaitic) varieties comprise the trend, and intermediate types are rare. In addition to nepheline and analcime, haüyne was observed in only three intrusions (Girod, 1971). The mafic mineralogy resembles that of the trachyte-rhyolite trend, but with rare phenocrysts of decayed brown amphibole observed in miaskitic trachyte and phonolite. Contrasting with the accessory titanite + apatite + zircon association of the miaskitic phonolites, the accessory mineral assemblage of the agpaitic phonolites (Azambre and Girod, 1966) includes rare minerals, such as aenigmatite, eudialyte, lavenite, rinkite (named 'mosandrite' in the original publication), and possibly rosenbuschite. Other rare minerals have yet to be identified.

GEOCHEMICAL EVOLUTION

Origin and Evolution of the Mafic Group of Rocks

Mafic lava flows and necks are easily distinguished in the field on the basis of their color. Dark-colored lava flows are ultrabasic to basic in composition (43%–47% SiO_2), with compatible trace element concentrations (Ni = 54–168 ppm, Cr = 70–284 ppm; Table 1) and MgO contents (6–8 wt %) that indicate relatively primitive compositions. The gray lava flows are more differentiated (47%–51% SiO_2) with lower contents of compatible trace elements (Table 1) and MgO contents < 5 wt%.

The Miocene and early Pliocene basanite plateau lavas and necks are Si-poor (43% SiO_2), fairly mafic, with an Mg# (Mg/[Mg + total Fe] atomic ratio) of ~0.50, and contain 85–110 ppm Ni and 180–220 ppm Cr. Though containing peridotite xenoliths and mantle-derived megacrysts, the most magnesian compositions are still not consistent with those of primary magmas, which should have Mg#s in the range 0.70–0.82. The magmatic rocks of the basanite-phonotephrite trend, with from 43% to 51% SiO_2, are saturated in olivine and clinopyroxene, suggesting that differentiation may have occurred at mantle depths during the Miocene and the early Pliocene.

Quaternary basanite-tephrite lava flows and necks are more silicic (47% SiO_2), but also more magnesian (Mg# of 0.51–0.56). They contain 80–170 ppm Ni and 215–280 ppm Cr. The magmas were multiply saturated but no really primitive compositions have been sampled. No differentiated rocks of the same age have been found.

Incompatible elements are abundant in all rock types, and their behaviors are roughly similar, implying nearly identical differentiation processes at depth. Rare earth element (REE)

contents range from 230 ppm in basanite to 660 ppm in phonotephrite; chondrite-normalized REE patterns (Figs. 6A–6B) are strongly fractionated; $(La/Yb)_N$ ranges from 20 to 40 without Eu anomalies, suggesting a garnet-bearing source and no plagioclase fractionation. Multi-element diagrams (Figs. 6C–6D) suggest derivation of the magmas from an enriched mantle source by fairly low degrees of partial melting. Primitive mantle–normalized trace-element patterns are strongly fractionated, with normalized abundances ranging from 125 to 500 (Ta, Nb) to 4–7 (Yb). The more highly incompatible large ion lithophile elements (LILEs), Rb, Ba, and Th, have normalized values between 50 and 100; K is slightly depleted in some samples. The less incompatible elements are increasingly depleted from 30 to 50 (P) down to 3–7 (Yb).

Evolutionary Trends in the Felsic Group of Rocks

The felsic and mafic trends are separated by a Daly gap in the 51–57 wt% SiO_2 range (Table 2). The felsic group of rocks shows two well-defined diverging trends in the TAS diagram (Fig. 4).

The silica-oversaturated trachyte-rhyolite trend, marked by increasing silica and slightly decreasing alkali contents, reflects alkali feldspar fractionation and late precipitation of quartz. Regarding incompatible trace element behaviors, two subgroups of rocks have been identified. Tamanrasset trachytes constitute the first subgroup, and Atakor trachytes-rhyolites, the second one.

The Tamanrasset trachytes are distinguished from the Atakor trachytes by their REE characteristics (Fig. 7A). REE contents vary from 300 to 500 ppm; REE patterns are strongly fractionated, with (La_N/Yb_N) of 27–12.5 and light (L) REE enrichment relative to heavy (H) REE. Eu anomalies vary from weakly positive (Eu/Eu* = 1.25 for 60.5 wt% SiO_2) to weakly negative (from Eu/Eu* = 0.80 at 61 wt% SiO_2 to 0.60 at 63 wt% SiO_2), with one exception of Eu/Eu* = 0.15, which corresponds to a more evolved (68 wt% SiO_2) sample with the highest REE content and the least fractionated REE pattern. Based on these data, it can be inferred that some Tamanrasset trachytes retain a cumulative feldspar component and that feldspar fractionation was delayed until SiO_2 reached ~61 wt%. In primitive mantle–normalized trace element patterns (Fig. 7D), strong fractionation from LILE (normalized values in the 100–1000 range, except Ba) to high field strength element (HFSE) (normalized values around 10 for Y and Yb) is obvious. In addition, weak to increasingly pronounced negative anomalies in Ba, Sr, P, Eu, and Ti (Figs. 7A–7D) provide evidence for incipient feldspar + apatite + Fe-Ti oxide fractionation.

Atakor trachytes-rhyolites have high total REE contents, varying widely from 630 ppm (62 wt% SiO_2) to 1000 ppm (66 wt% SiO_2) to 375 ppm (68 wt% SiO_2) to 200 ppm (72 wt% SiO_2). REE are incompatible in trachytic liquids until the trachyte-rhyolite boundary is reached, where they ultimately become compatible, probably because of apatite + zircon fractionation, as evidenced by decreasing amounts of P_2O_5, Zr, and Hf. LREE patterns are
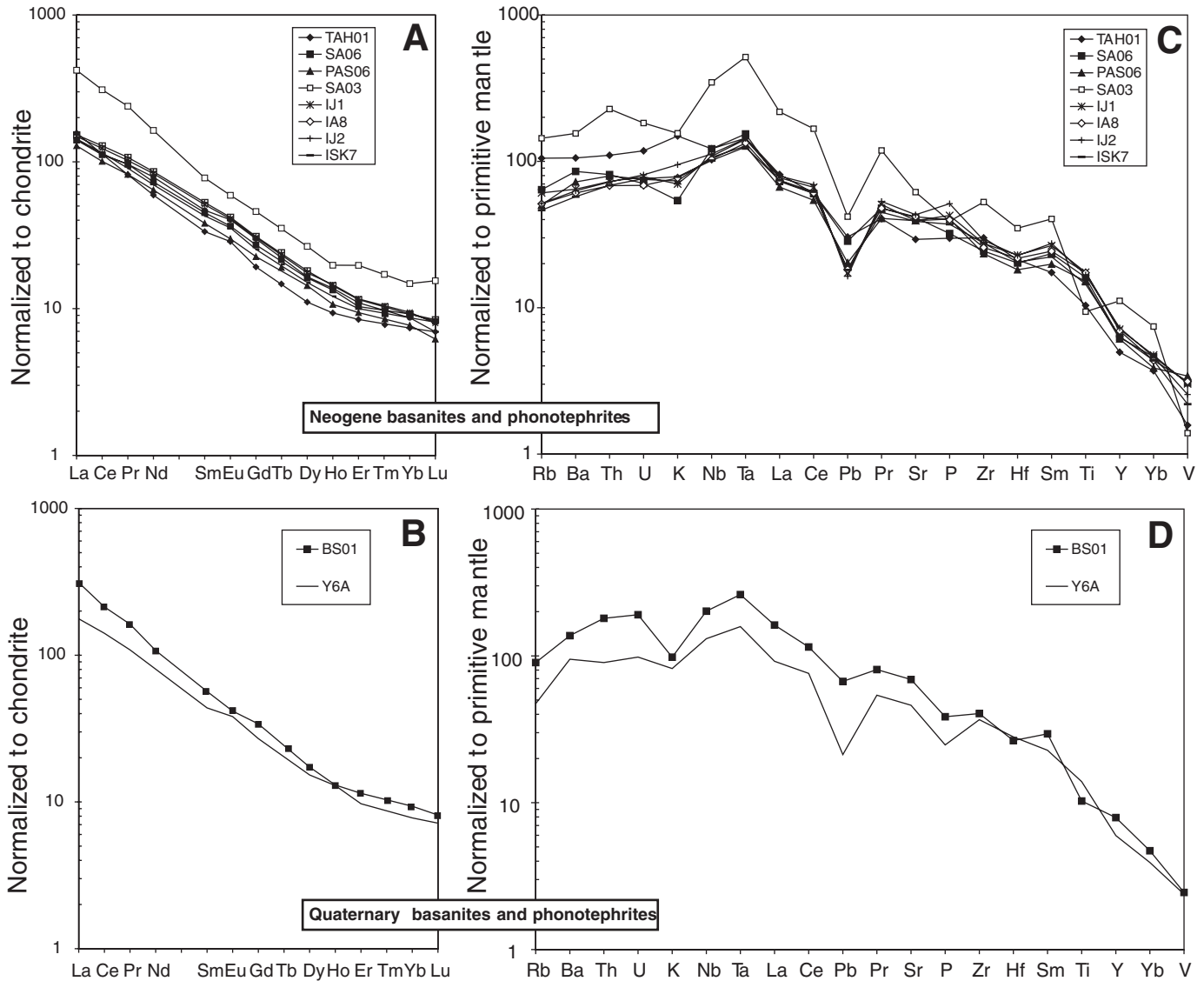
Figure 6. Geochemical characteristics of the mafic group of rocks. (A) Rare earth element (REE) patterns of Neogene rocks (normalization values of McDonough and Sun, 1995). (B) REE patterns of Quaternary rocks. (C) Primitive mantle–normalized multi-element patterns of Neogene rocks (normalization constants from Sun and McDonough, 1989, updated in McDonough et al., 1992). (D) Primitive mantle–normalized multi-element patterns of Quaternary rocks.

slightly fractionated (Fig. 7B), with no HREE fractionation, but with deep negative Eu anomalies. Eu/Eu* values range from 0.5 to 0.1 in the trachytes down to 0.04 in the rhyolites, indicating extensive feldspar fractionation. Primitive mantle–normalized trace-element patterns (Fig. 7D) show that K is depleted relative to U and Ta. As a continuation of the incipient fractionation processes observed within the Tamanrasset trachytes, deep troughs in Ba, Sr, P, Ti, and Eu (Figs. 7 B–7D) are conspicuous in the trace-element patterns of the high-silica trachyte and rhyolite. Other incompatible elements can reach extremely high normalized values, e.g., around 1000 for Th, U, Ta, and Nb in rhyolite.

The silica-oversaturated trachyte-rhyolite trend is characterized by very high Y + Nb values and plots in the within-plate granite (WPG) field (Pearce et al., 1984). Extremely low (less than 0.3) Y/Nb ratios correspond to the A1 group of A-type granites (Eby, 1992), which are considered to be representative of rift and/or hotspot tectonic settings.

The more complex silica-undersaturated trachyte-phonolite trend involves two steps in the TAS diagram (Fig. 4). The first step, which has both increasing silica and alkali contents, is illustrated by the metaluminous (miaskitic) subgroup. The second step, which has decoupled behaviors of silica (decreasing contents) and alkalis (increasing contents), characterizes the peralkaline (agpaitic) subgroup, which has a highly sodic, silica-poor mineralogy. The two-step trend is well expressed in diagrams of differentiation index (DI), defined as the sum of
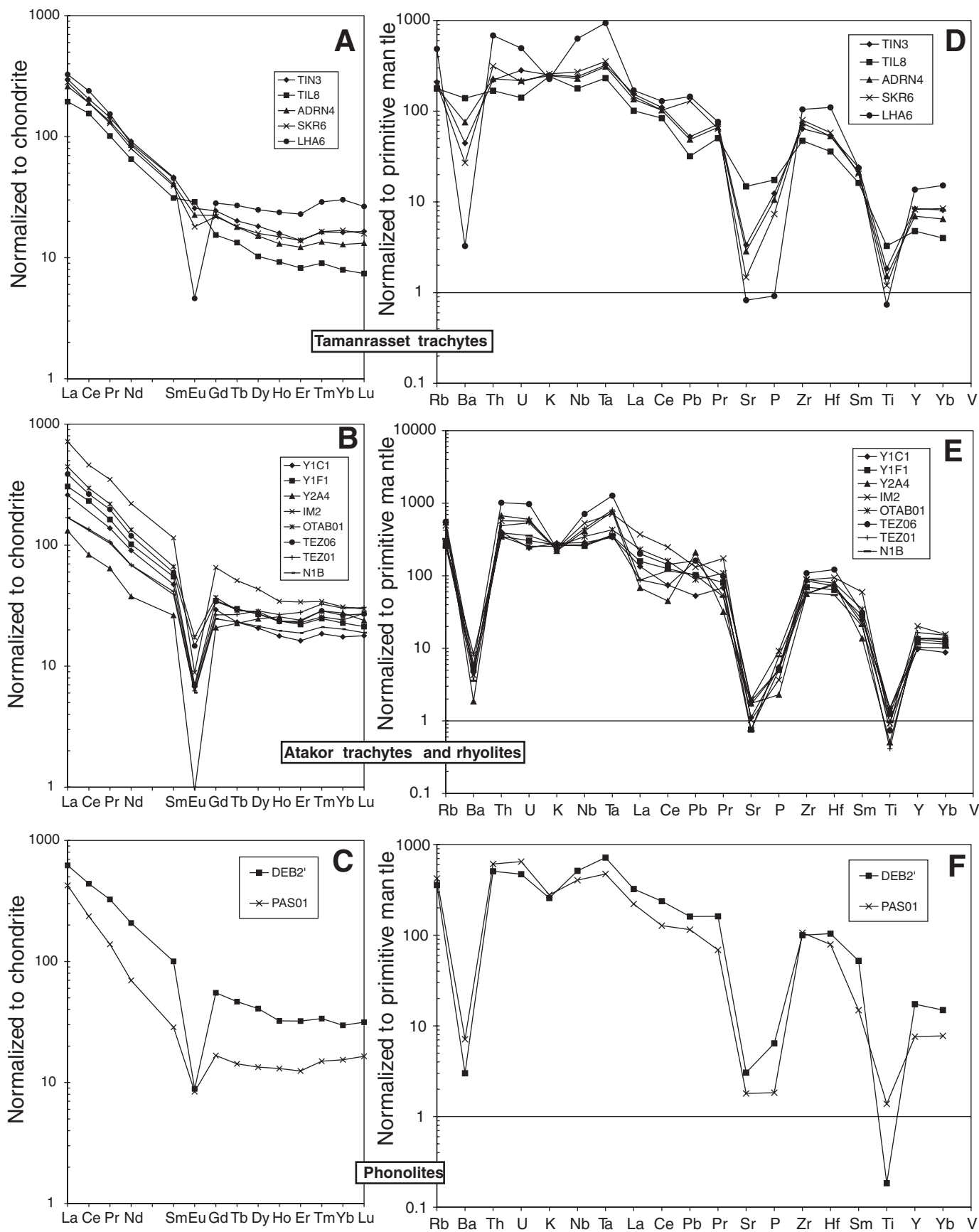
Figure 7. Geochemical characteristics of the felsic group of rocks. (A) Rare earth element (REE) patterns of Tamanrasset trachytes. (B) REE patterns of Atakor trachytes and rhyolites. (C) REE patterns of phonolites. (D) Primitive mantle–normalized multi-element patterns of Tamanrasset trachytes. (E) Primitive mantle–normalized multi-element patterns of Atakor trachytes and rhyolites. (F) Primitive mantle–normalized multi-element patterns of phonolites.

CIPW-normative orthoclase + albite + quartz + nepheline, versus CIPW-normative nepheline (Fig. 8A). In peralkaline rocks, Na_2O in excess of Al_2O_3 is converted into CIPW-normative acmite (Ac) and sodium disilicate (Ns), which are not considered in the DI calculation. The two steps remain well defined in a diagram combining DI and (Ac + Ns) (Fig. 8B). Phonolites are poorly represented in our data set, and only two agpaitic types were sampled. REE contents and patterns resemble those of the trachyte-rhyolite trend, with fractionated LREE, negative Eu anomalies (Eu/Eu* of 0.25–0.1), and no HREE fractionation (Fig. 7C). Primitive mantle–normalized trace-element patterns (Fig. 7E) do not show such extreme enrichments as in the rhyolites, but their shapes suggest similar sources and processes.

DISCUSSION

The Atakor massif is located within the Hoggar province, which constitutes part of the large Tuareg shield in the north-central part of West Africa (Black et al., 1994). While some Cenozoic volcanic provinces within the African continent (Liégeois et al., 2005) are clearly within-plate in character, e.g., Hoggar, Libya, Tibesti, and Darfur, others are related to plate boundaries,

Figure 8. Selected trachyte-phonolite compositions, recalculated on H_2O- and CO_2-free basis, using same symbols as in Figure 4. CIPW-normative Ne versus differentiation index (DI) diagram and CIPW-normative Ne versus (DI + Ac + Ns) diagram.

e.g., East African Rift and Ethiopia, Cameroon line (Fitton, 1987), Cabo Verde archipelago and Canary Islands, and the Maghreb (Lustrino, 2000; Savelli, 2002). The association of topographic swells and Cenozoic volcanism is remarkable, and to account for the relationships among within-plate volcanic activity, topographic elevation, and mantle seismic velocity anomalies, the involvement of one or several mantle plumes has been suggested (for contrasting views, see Burke, 1996; Liégeois et al., 2005; Pik et al., 2006). The popular plume model postulates that hot mantle material upwelling from the lower mantle impinged on the base of the Tuareg shield lithosphere and induced partial melting of either the subcontinental lithospheric mantle, or the plume itself, or a mixture of both (e.g., Aït-Hamou et al., 2000).

The Cenozoic evolution of the Tuareg shield has to be considered in the context of the motion of the African plate. As noted by Frizon de Lamotte (2006), Africa is almost entirely (90%) surrounded by passive continental margins, with the Afar triple junction commonly regarded as plume-related. The only exception is the Mediterranean region (Fig. 1), where Africa-Eurasia convergence has been accommodated since the Cretaceous either by subduction, a process that occurs now only in the Eastern Mediterranean, or by transcurrent and thrust faults that are currently active in the Western Mediterranean. The stresses at convergent plate boundaries are higher, by several orders of magnitude, than those at passive continental margins, as illustrated by the current low levels of seismicity along the coastlines of Africa compared with the Atlas belt of Morocco (Sébrier et al., 2006), and the Maghreb in general. The Tuareg shield is only 1000 km south of the Mediterranean coast (Fig. 1). In the case of within-plate igneous activity, the role played by events occurring at nearby plate margins should be envisaged as an alternative possibility to mantle plumes of deep origin (Anderson, 2005). The plate tectonics paradigm predicts that the Hoggar volcanic activity and reactivation of Precambrian fault systems are likely to be more closely related to geodynamic events occurring in the Mediterranean region than at more remote, passive plate margins.

In the following discussion, we examine the nature and composition of the upper-mantle sources of the magmatism, and the periodicity of the volcanic activity, discuss the various models that might explain how magmas can be generated in this within-plate tectonic setting, and the temporal relationships with the geodynamic evolution of the Western Mediterranean.

Upper Mantle Sources of the Cenozoic Magmas

The primitive mantle–normalized multi-element patterns of the mafic rocks of the Atakor massif are highly enriched in incompatible elements (Fig. 6), similar to the HIMU (high μ) end member of the oceanic-island basalt (OIB) spectrum (Weaver 1991a, 1991b). This observation is consistent with Sr-Nd-Pb isotope characteristics of the Atakor basalts (Allègre et al., 1981; Dupuy et al., 1993), which indicate a HIMU affinity for the mantle source.

The temperature and depth (or pressure) at which the mafic magmas segregated from their mantle sources can be calcu-

lated based on empirical equations, with statistical uncertainties of ±40 °C and ±8 km (or ±0.27 GPa) (e.g., Albarède, 1992). Removal of clinopyroxene can shift the calculated temperature and pressure by ~5–10 °C and 0.1–0.3 GPa. In the following estimations, the more differentiated mafic magmatic rocks with low Ni and Cr contents have been discarded. The Ni- and Cr-rich, more magnesian, and least siliceous Miocene-Pliocene basanite magmas could have segregated from their mantle source at temperatures of 1260–1270 ± 40 °C and pressures of 1.9–2.2 ± 0.27 GPa, corresponding to depths of ~55–65 ± 8 km, i.e., within the subcontinental lithospheric mantle. The temperature and pressure of segregation of the more primitive Quaternary basanite-tephrite magmas are estimated at 1250 ± 40 °C and 1.3 ± 0.27 GPa, corresponding to a depth of 40 ± 8 km, close to the crust-mantle boundary, but still within the subcontinental lithospheric mantle.
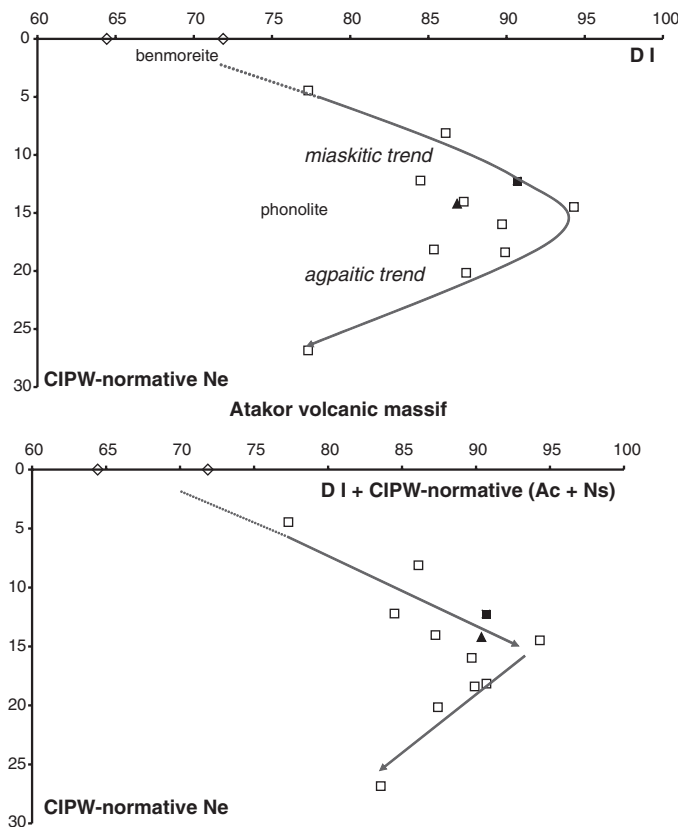
These values are surprisingly low for silica-deficient mafic lavas, which are commonly considered to be generated at considerably greater depths. In the nearby Tahalra massif (Dautria et al., 1988), low-Ni, low-Cr Miocene basanites are clearly differentiated, but one primitive Miocene sample yields a depth of 105 ± 8 km. High-Ni, high-Cr Quaternary alkali basalts yield comparable depths of 110 ± 8 km. Because these preliminary calculations indicate that the mafic magmas of the Atakor and Tahalra massifs differ in terms of their calculated segregation depths, a further 17 mafic rock compositions previously reported by Girod (1971) were also considered. These data are not directly comparable with our data, because they were obtained by wet chemical analysis and no Ni and Cr abundances were reported. For 14 of Girod's samples, calculated depths vary from 35 to 80 ± 8 km, which is in agreement with our results. The other three high-Mg, low-Si compositions yield greater depths of 92–100 ± 8 km. Girod (1971) noted that these three compositions correspond to Miocene basanites crowded with olivine phenocrysts (limburgitic facies). If the olivine phenocrysts were accumulative, the resultant whole-rock compositions would have lower SiO_2 and higher MgO contents compared with the true parent magmas, and thus the apparently greater depth of magma segregation could be an artifact. Consequently, we do not consider the calculated 92–100 km depths to be meaningful.

Thus, the Atakor Neogene mafic magmas indicate fairly shallow depths of segregation compared to the Tahalra Quaternary basanite magmas (Dautria et al., 1988), which segregated at ~110 km. A possible explanation could be that the Atakor magmas have experienced some low-pressure differentiation, such that the calculated depths are not meaningful in terms of magma segregation processes. However, the Ni and Cr contents of the samples selected for the calculations are in the range of 110–170 ppm and 220–280 ppm, respectively, which are similar to those of the Tahalra basanites. A second possibility could be that the Atakor magmas did actually segregate at shallower depths than the Tahalra magmas, suggesting that different magma generation processes operate within the subcontinental lithospheric upper mantle. In the Tazrouk massif, located to the northeast of the Atakor massif, a basanite has also indicated an intermediate depth of segregation of 80 ±

8 km (work in progress). A third possibility would be that the mafic magmas originated from different upper-mantle sources. The least differentiated, noncumulative mafic lavas have Mg# ranging in the Tahalra massif from 0.57 to 0.69 in basanites, 0.41–0.53 in alkali basalts (Dautria et al., 1988), and in the Atakor massif from 0.50 to 0.56 in Neogene basanites. Samples with primitive Mg#, i.e., 0.70 – 0.82, have not been identified anywhere, implying that none of the mafic magmatic rocks represents unmodified partial melts of mantle peridotite.

The Sr-Nd-Pb isotope systematics of the alkali basalts, basanites, and nephelinites from the Hoggar alkaline volcanic province (Allègre et al., 1981) are consistent with their generation from a HIMU-type mantle source; they have $^{87}Sr/^{86}Sr$ ranging from 0.70310 to 0.70348, $\varepsilon_{Nd(t)}$ varying from +4.5 to +6.9 ± 0.8, and high Pb isotopic ratios ($^{206}Pb/^{204}Pb$ up to 20.373 ± 0.014, and $^{207}Pb/^{204}Pb$ up to 15.696 ± 0.017 for a nephelinite). This range of compositions, confirmed subsequently by Dupuy et al. (1993), shows that the source of the Neogene magmas is not strongly depleted. The HIMU isotopic signature of the mafic magmatic rocks is consistent with their incompatible trace element patterns (Fig. 6).

Episodic Nature of the Igneous Activity in the Hoggar Province

The Atakor massif, located on top of a major topographic swell, was active only during the more recent magmatic episodes of the Hoggar volcanic province. The first, Burdigalian, episode in the Atakor massif occurred ca. 20 Ma, while the Hoggar province as a whole began to erupt at the Eocene-Oligocene boundary, ca. 34 Ma. Though reliable isotopic age determinations are scarce, they provide a general framework for considering the spatial and temporal variations in the characteristics of the Cenozoic volcanism.

The first volcanic episode, located in the Anahef province, was marked by outpouring of a thick pile of flood basalt lavas in the Taharaq district (Aït-Hamou, 2000). A highly eroded 300–700-m-high plateau is composed of a sequence of 5–10-m-thick lava flows. Its original area probably covered around 1500 km^2, and the total thickness of the eruptive sequence could have been as much as 1500 m. The volume of preserved flood basalts is ~200 km^3, although the original volume has been estimated at 1000 km^3, and could have been as high as 2000 km^3. Preliminary K-Ar determinations have suggested a long-lasting volcanic episode from 44 ± 0.8–24.4 ± 0.5 Ma (Lutetian to Chattian), with a good correlation between the topographic elevation of the magmatic rocks and their isotopic ages. The same samples when dated by the ^{40}Ar-^{39}Ar method yield identical, though less precise, ages, ranging from 34.5 ± 3.5 Ma to 32.8 ± 2.6 Ma, corresponding to the Eocene-Oligocene boundary, i.e., from Priabonian to Rupelian (Aït-Hamou et al., 2000). Younger K-Ar ages, from 28.5 ± 0.5 Ma to 24.4 ± 0.5 Ma are regarded, at least partly, as the result of the thermal effects of intrusion of 29–24 Ma alkaline ring complexes (Maza et al., 1998). The lavas are mainly high-K, high-P, high-Ti (HKPT) tholeiitic basalts with subordinate amounts of alkaline

rocks ranging from alkali basalt to trachyandesite. No low-K, low-P, low-Ti (LKPT) basalts, characteristic of many continental flood basalt provinces, have been sampled so far. Using only the high-Ni (110–363 ppm), high-Cr (210–698 ppm) unaltered mafic rocks, the calculated depths of segregation of the olivine tholeiitic basalt magmas range from 73 to 38 ± 8 km. Cumulative rocks (ankaramites) yield a similar range of depths from 61 to 44 ± 8 km. The factors controlling the calculated segregation depths are mostly the Mg#, and to a lesser extent the Ni and Cr contents; the greatest depths correspond to a Mg# of 69 and the highest Ni and Cr contents, while the shallowest depths correspond to Mg# of ~50–55, with but varying abundances of Ni and Cr. Sr-Nd-Pb isotope systematics (Aït-Hamou et al., 2000) do not identify a single source for the magmatism, but rather a heterogeneous source varying between HIMU and EM1 (enriched mantle) end-member characteristics, with $^{87}Sr/^{86}Sr$ from 0.703544 to 0.704519, $^{143}Nd/^{144}Nd$ from 0.512522 to 0.512796, $^{206}Pb/^{204}Pb$ from 18.361 to 19.499, and $^{207}Pb/^{204}Pb$ from 15.580 to 15.624.

The second magmatic episode is located nearly at the same place as the Taharaq district, and it consists of plutonic ring complexes and associated volcanic formations (Rémy, 1967; Maza, 1998). Radial dike swarms also occur; these were emplaced at shallow (~500 m) depths within the 34 Ma tholeiitic flood basalt pile. The magmatic rocks are classified into a restricted suite of older tholeiitic olivine gabbros, yielding a K-Ar age of 29 ± 0.6 Ma (late Rupelian), and a younger compositionally more variable alkaline suite of essexite, monzonite, and syenite. Extrusions of late trachyte and peralkaline rhyolite yield a K-Ar age of 24 ± 0.4 Ma (late Chattian). Field relationships between the unroofed plutonic ring complexes and the late extrusive volcanic deposits indicate that between 29 and 24 Ma, the Anahef area experienced an uplift rate of ~0.4 mm yr⁻¹. The Sr-Nd-Pb isotope systematics of the magmatic rocks (Maza et al., 1998) indicate a variety of sources, with the tholeiitic plutonic rocks having isotopic compositions between those of the EM1 and HIMU mantle end members, while the alkaline plutonic rocks cluster near the HIMU end member, and the rhyolite plots in an intermediate position between EM1 and HIMU. The available isotopic data suggest a shift from a heterogeneous mantle source in the Oligocene to a more homogeneous Miocene to Quaternary HIMU-like source.

Following this second magmatic episode, alkaline magmatism occurred throughout the Hoggar swell. North of the Taharaq flood basalt province, the magmatism of the Serouenout district includes nephelinite, basanite, trachyte, and phonolite, with a pronounced Daly gap between 42 and 58 wt% SiO_2 (Maza, 1998). The most primitive compositions yield magma segregation depths of 96–100 ± 8 km for basanite and 139–183 ± 8 km for nephelinite. While the Mg# is the prime indicator of magma segregation depth for each magma type, for the same Mg#, nephelinite magma was segregated significantly deeper than basanite magma, e.g., for a Mg# of 0.58, the calculated depths are 139 and 96 km, respectively. These calculated magma segregation depths are by far the highest in the entire Hoggar volcanic province. The age of the eruptions in the Serouenout district is not known precisely, though it is likely to be Miocene and coeval with the first volcanic episode in the Atakor massif.

In summary, the Hoggar volcanic province was the site of repeated volcanic episodes, separated by periods of quiescence. According to currently available data, it is possible to distinguish six eruptive episodes:

1. The first episode is Oligocene in age, ca. 34–32 Ma, and is characterized by the outpouring in the Taharaq district of a thick sequence of HKPT tholeiitic flood basalts, with a total volume estimated at 1000–2000 km³.

2. The second episode is marked by emplacement at shallow depths (probably as low as 500 m) of tholeiitic to alkaline ring complexes, ca. 29 Ma, in the same area as the older flood basalts.

3. The third episode corresponds to the emplacement, ca. 24 Ma, of silicic extrusions (trachyte and peralkaline rhyolite) on top of unroofed alkaline ring complexes, indicating uplift rates of ~0.4 mm yr⁻¹ within the Taharaq district.

4. The different eruptive episodes in the Atakor massif have occurred since 20 Ma. The first episode, actually the fourth episode in the Hoggar, lasted from 20 to 12 Ma, with the outpouring of alkaline flood basalts and associated intermediate pyroclastic formations, and it ended with the emplacement of large phonolite domes and lava flows. The subsequent episode, i.e., the fifth episode in the Hoggar, was shorter, between 6.7 and 4.2 Ma, with eruptions of a compositionally variable bimodal suite of basanite to phonotephrite and benmoreite to trachyte, phonolite, and scarce rhyolite. The last episode, i.e., the sixth episode in the Hoggar, began 1.9 Ma and lasted until the present, with exclusively basanite lava flows and associated scoria cones. The Tahalra massif has also yielded Pliocene–Quaternary ages from 3.5 Ma (unpublished data referred to in Aït-Hamou et al., 2000).

Since the Eocene-Oligocene boundary, igneous activity in the Hoggar massif has not been continuous, but periodic. The six periods of igneous activity differ in their duration, ranging from less than 1 m.y. (the oldest episodes) up to 7 m.y. (the Miocene episode of Atakor). The five intermediate periods of quiescence have durations of ~2–5 m.y.

Magma-Generating Dynamic Processes

In the mantle below the Hoggar swell, Neogene HIMU-like mantle sources appear to have replaced an Oligocene mixed source, involving both HIMU and EM1 end members (Aït-Hamou et al., 2000). Sr-Nd-Pb isotopic variations, coupled with the shift at 29 Ma from tholeiitic to alkaline igneous activity, are commonly explained by the involvement of a deep mantle plume. The popular "plume" model postulates that hot materials coming from the lower mantle impinged on the base of the lithosphere and induced partial melting of either the subcontinental lithospheric mantle, or the interior of the plume itself, or a mixture of both. Allègre et al. (1981) suggested that the HIMU source of OIBs originated from the lower mantle, whereas the heterogeneous sources for intracontinental flood basalts were located within the subcontinental lithospheric upper mantle. Aït-Hamou et al. (2000) adopted this

model, stating that the isotopic signature of the tholeiites suggests that they were derived from a heterogeneous mantle source dominated by a lithospheric component near the EM1 end member, and that the subsequent alkali lavas required the involvement of a near end-member HIMU component of possible plume origin. Such a scenario can be challenged, and these authors admit that the nature and origin of the two enriched mantle end members have yet to be defined, as both components could be lithospheric, or, equally, could have a deeper origin.

Alternatively, a scenario combining an EM1-like plume component and a HIMU-like subcontinental lithospheric mantle source is tenable: the first, short-lived episode would imply fairly high degrees of partial melting (tholeiitic basalt magmas) of both plume and lithosphere materials, and the subsequent, long-lasting episodes would be marked by fairly low degrees of partial melting (basanite magmas) of the lithospheric mantle. Whether the HIMU sources are located in deep peridotitic mantle, or in garnet pyroxenite-bearing lithospheric mantle, is a highly debated issue (e.g., Hirschmann et al., 2003; Niu and O'Hara, 2003).

Any discussion dealing with the plume concept is biased because the term "plume" is frequently defined in a very loose manner. Volcanic provinces are considered as "hotspots" fuelled by mantle plumes coming from below, but the origin of the thermal anomalies is a major issue for debate (e.g., Courtillot et al., 2003; Anderson and Natland, 2005). In the original plume theory, mantle plumes were inferred to come from great depths, possibly down to the core-mantle boundary, plume heads were large-scale features (~1000 km in diameter), inferred to trigger continental flood basalt magmatism, and smaller wavelength convective instabilities were not considered as real plumes. The two types of upwelling materials were expected to sample deep and shallow mantle regions, respectively.

To define a mantle plume requires that several specific features be recognized. The major geochemical argument used currently to support a deep mantle origin is the occurrence in the lavas of high $^3He/^4He$ ratios, though this argument has been questioned (Anderson, 2001). A compilation of new helium isotope results throughout Africa (Pik et al., 2006) indicates that the magmatism of the Ethiopia-Afar province could originate from a large, deep-rooted mantle plume characterized by a high ^3He signature, possibly originating from the core-mantle boundary according to seismic tomography data. All other African intraplate volcanic provinces, including the Miocene basanites of the central Atakor massif, are more likely linked to a second-order type of shallow-mantle upwelling, presumably originating from depths shallower than 400 km, as suggested by seismic wave imaging (Sebai et al., 2006).

In the Tuareg shield, the lithospheric thickness varies significantly from west to east (Liégeois et al., 2005), i.e., from ~100 km west of 4°50E (corresponding to juvenile Pan-African terranes), to ~160 km between 4°50E and 8°30E (older reworked terranes, including Laouni, Azrou-n-Fad, Tefedest, Egere-Aleksod, grouped into the LATEA microcontinent, Fig. 9), and to no more than 100 km east of 8°30E (East Saharan meta-

craton). The initiation of igneous activity could have been facilitated by edge-driven small-scale convection, induced by strong lateral temperature gradients (King and Anderson, 1998).

Magma segregation depths along the major axis of the Hoggar swell are apparently unrelated to lithosphere thickness. In the southwest to northeast transect, the following values have been calculated from available data for Neogene alkali basalts and basanites: ~110 km in Tahalra, ~65–40 km in Atakor, ~80 km in Tazrouq, and ~100 km in Serouenout. Taharaq Oligocene tholeiitic basalts yield depths of ~75–40 km, and Serouenout Miocene (?) nephelinite magmas segregated at depths from 140 up to 180 km. With the exception of the Serouenout nephelinites, all the computed depths are shallower than the LATEA lithospheric thickness of 160 km, implying that the magmas segregated from mantle sources within the subcontinental lithosphere. Additionally, those volcanic districts emplaced within major Precambrian shear zones yield the lowest values.

Periodic igneous activity in the Hoggar province is inconsistent with a single event of hot material intrusion at the Eocene-Oligocene boundary. No negative shear-velocity anomalies, diagnostic of thermal perturbations, have been detected above 250 km depth below the Tuareg shield (e.g., Figure 7E of Ritsema, 2005). The fairly shallow depths computed for magma segregation need to be reconciled with the apparently normal heat flow in the Hoggar province (Lesquer et al., 1989) and seismic tomography data indicating fast wave velocities (Shapiro and Ritzwoller, 2002). Ayadi et al. (2000) identified only weak velocity contrasts below Tahalra and Atakor. This paradox would seem to indicate that each thermal event related to magma segregation, ascent, and emplacement was short-lived enough to prevent the development of long-lasting thermal anomalies in the mantle beneath the Hoggar swell.

Consequently, we suggest that the periodic igneous activity of the Hoggar is related to episodic fault activity. High fault stress and low lithospheric stiffness favor large variations of slip rates along fault zones (Chéry and Vernant, 2006). In an elastic lithosphere loaded by plate motion, a low-loading velocity causes fault-slip rates to cycle between high and low values, while a high-loading velocity leads to low stress and constant slip rates. The African and Eurasian continental plates have been converging since the Cretaceous. Periods of low-velocity plate motion could, therefore, have promoted reactivation of remote fault zones and triggered episodic igneous activity.

The various volcanic districts in the Hoggar province, especially the Atakor massif, are closely associated spatially with Pan-African basement lineaments dissecting the Tuareg shield that were rejuvenated as brittle faults during the Paleozoic and the Mesozoic. The slip rates along those fault zones reactivated during the Cenozoic have yet to be determined. Liégeois et al. (2005) argued that mantle decompression melting and resulting igneous activity could have taken place during local and short-lived episodes of fault reactivation along weakness zones, which induced near-vertical lithosphere delamination (Fig. 9). Generation of OIB-like magmas is a function of the degree of partial melting, the size of the melting zone, and the length scales of
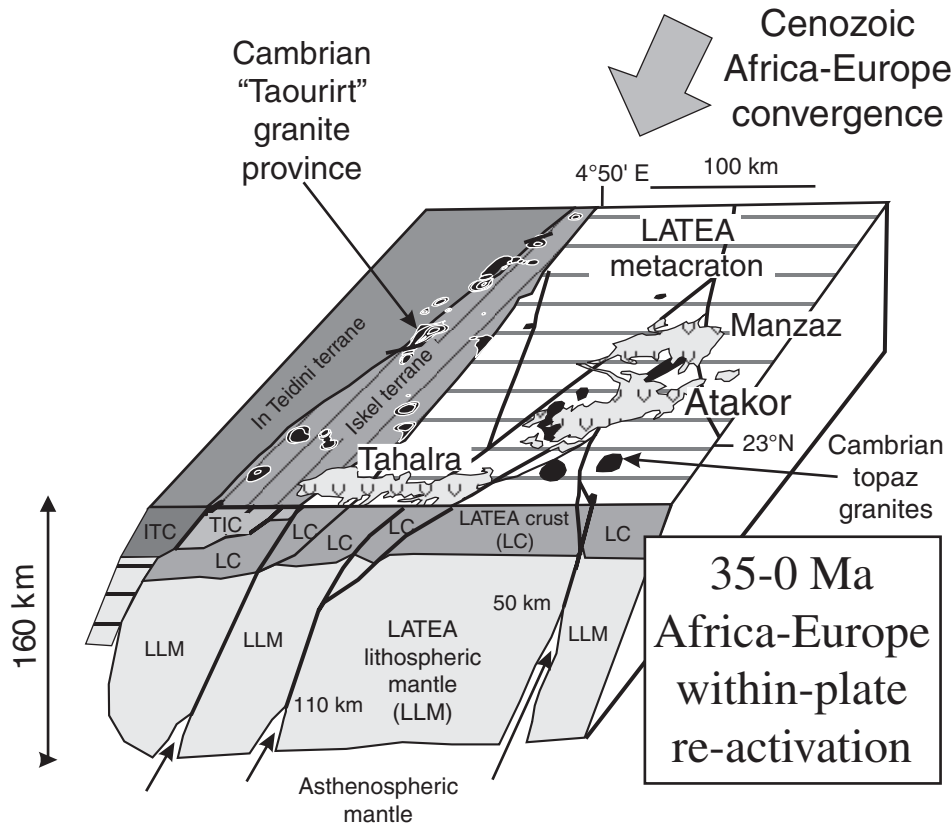
Figure 9. Delamination model for the Hoggar Cenozoic magmatism (after Liégeois et al., 2005).

mantle heterogeneity (Meibom and Anderson, 2004). Linear delamination along shear zones can explain how melt segregation depths, and possibly even melt generation zones, can be shallower than expected in a regionally thick lithosphere.

Relations with the Evolution of the Western Mediterranean

The Hoggar massif, including the Atakor massif, remained remarkably stable tectonically for a period of ~500 m.y., i.e., since the Cambrian, when the 525 Ma topaz granites (Cheilletz et al., 1992) of the "Taourirt" granite province (Azzouni-Sekkal et al., 2003) were emplaced (Fig. 2). The origin of Cenozoic fault reactivation remains obscure if only local data are considered. Africa-Eurasia convergence since the Cretaceous has resulted in the formation of the Alpine orogenic belt through subduction, shortening, and uplift, and the formation of small oceanic basins in the Western Mediterranean through microplate rotation, extension, and subsidence. What has happened since the Eocene-Oligocene boundary in the Hoggar province is worth considering in relation to global geodynamic events.

The Paleogene in the Hoggar is marked by three Oligocene volcanic episodes at 34, 29, and 24 Ma. No Eocene igneous episodes are known so far. In the Mediterranean area (Fig. 1), Eocene times represent a transition from a period dominated by Iberia-

Eurasia convergence, with the formation of the Pyrenees-Provençe mountain range, to a period dominated by Apulia-Eurasia convergence, leading to the formation of the Alpine mountain range, during which time the major plate boundary between Africa and Eurasia was initiated, characterized by a northward-dipping subduction system. The African continent was still separated from the Eurasian continent by remnants of subducting Neotethys oceanic basins, and no high stress fields were applied to the continental passive margin. The period from 35 to 30 Ma was a key one (Jolivet and Faccenna, 2000), because it marked the onset of full collision between Africa and Eurasia and the inception of backarc extension in the whole region. At 30 Ma, the subduction regime changed from compressional to extensional in the whole Mediterranean region, as a consequence of continental collision and the slowing down of the northward motion of Africa. Slow plate velocities could have promoted reactivation of a specific Precambrian fault zone in the Hoggar that formed the boundary between the Serouenout and LATEA terranes. Periodic linear delamination of the lithospheric mantle in the fault zone triggered, successively, the development at 34 Ma of a large volume of tholeiitic flood basalts, the emplacement at 29 Ma of tholeiitic to alkaline ring complexes, and finally the extrusion at 24 Ma of silicic peralkaline volcanic rocks. The 29 Ma ring complexes illustrate the rapid shift (Maza et al., 1998) from tholeiitic magmas, derived by partial melting of a heterogeneous mantle source (Aït-Hamou et al., 2000), to

alkaline magmas from a more homogeneous HIMU-like source, suggesting that any thermal anomaly associated with the origin of the 34 Ma flood basalts must have disappeared progressively in a 5 m.y. period of time.

The Neogene was marked by the closure of the last Neo-tethys basins between Africa and Eurasia, which was completed by 21 Ma (Rosenbaum et al., 2002). Since then, the Atakor massif experienced three volcanic episodes, separated by long-lasting periods of quiescence. These episodes reflect the complex evolution of the Western Mediterranean, with the formation of three backarc basins. The first volcanic episode in the Atakor massif is nearly coeval with extensional events initiating, successively, the 25–23 Ma Valencia trough between Iberia and the Balearic Islands, the 21–18 Ma oceanic Algero-Provençal Basin, and the 18–10 Ma Alboran Sea. The following period of quiescence in the Atakor massif was marked by extensive igneous activity within the Western Mediterranean area, especially in the Rif-Tell fold belts of the Maghreb (Maury et al., 2000, and references therein), where discrete igneous episodes correspond to slab breakoff and abrupt changes in the kinematics of Africa-Eurasia plate convergence (Rosenbaum et al., 2002). It is remarkable that the major tectonic episodes in the Rif-Tell fold belt were apparently not accompanied by volcanic activity in the Atakor massif. More isotopic age determinations are necessary to substantiate whether this period of time was really quiescent, or not. The second volcanic episode in the Atakor massif was coeval with the extensional event that created the northern part of the Tyrrhenian Sea, floored by thinned continental crust, and isolated Corsica from the central Italian mainland. The following period of quiescence in the Atakor massif ended with the inception of the two deep oceanic basins in the southern part of the Tyrrhenian Sea, isolating Sardinia from southern Italian mainland and Sicily.

To sum up, episodes of igneous activity in the Hoggar swell appear to have been nearly coeval with extensional events in the Western Mediterranean, inducing relaxation of boundary stress fields caused by low-plate-loading velocities, while periods of quiescence could correspond to compressional events, inducing a high-stress regime and a high-plate-loading velocity.

SUMMARY AND CONCLUSIONS

The Atakor massif is located at the center of the Hoggar swell within the Tuareg shield. It is characterized by volcanic activity during three discrete Neogene igneous episodes, separated by fairly long periods of quiescence. The topographic highs are composed of Precambrian basement uplifted since the Pliocene and of overlying lava plateaus, domes and spines, scoria cones, and valley-filling lava flows. The mantle source of the magmas has a dominant HIMU-like characteristic, with a K-poor signature and significant incompatible element enrichment showing LILE to HFSE fractionation.

The magmatic rocks have been subdivided into two groups with contrasting compositions. The mafic group includes a Miocene–Pliocene basanite-phonotephrite trend and a subsequent Pliocene–Quaternary basanite-tephrite association. Peridotite mantle xenoliths and megacrysts (kaersutite, mica, diopside, zircon, oxides, etc.) indicate that magmatic differentiation processes must have operated within the upper mantle up to the crust-mantle boundary. The felsic group, separated by a Daly gap from the mafic lavas, is compositionally more variable with two diverging trends, a silica-saturated to oversaturated benmoreite-trachyte-rhyolite trend with metaluminous, peralkaline, and scarce peraluminous varieties, and a silica-undersaturated trachyte-phonolite trend with metaluminous (miaskitic) and peralkaline (agpaitic) varieties. The more evolved magma compositions indicate magmatic differentiation involving feldspars, apatite, zircon, and Fe-Ti oxides.

The depths of melt segregation of the most primitive mafic magmas in the Hoggar vary from ~110 km in Tahalra to ~65–40 km in Atakor, with intermediate values of ~75–40 km (Taharaq), ~80 km (Tazrouq), and ~100 km (Serouenout). These calculated depths are shallower than the LATEA (corresponding to the Laouni, Azrou-n-Fad, Tefedest and Egere-Aleksod terranes) lithospheric thickness of 160 km. These apparently contradictory results can be reconciled if we consider the possibility that magmatism was triggered by lithospheric delamination along linear shear zones, allowing the ascent and decompression partial melting of the asthenospheric mantle. The extent of asthenospheric ascent was more or less significant according to the magmatic period and the location of the igneous activity.

The episodic nature of the volcanic activity can be related to episodic large-scale tectonic events occurring at the Africa-Eurasia convergence boundary in the Western Mediterranean. The discrete magmatic episodes were likely triggered by a drastic slowing down in the motion of the African plate, which induced major changes in the stress regime and caused reactivation of pre-existing Precambrian faults.

REFERENCES CITED

Aït Hamou, F., 2000. Un exemple de "point chaud" intra-continental en contexte de plaque quasi-stationnaire: Étude pétrologique et géochimique du Djebel Taharaq et évolution du volcanisme Cénozoïque de l'Ahaggar (Sahara Algérien) [Thèse de Doctorat en Sciences]: Montpellier, Université Montpellier II–Sciences et Techniques du Languedoc, 200 p.

Aït-Hamou, F., Dautria, J.M., Cantagrel, J.M., Dostal, J., and Briqueu, L., 2000, Nouvelles données géochronologiques et isotopiques sur le volcanisme Cénozoïque de l'Ahaggar (Sahara Algérien): Des arguments en faveur d'un panache: Comptes Rendus de l'Académie des Sciences de Paris, v. 330, p. 829–836.

Albarède, F., 1992, How deep do common basaltic magmas form and differentiate?: Journal of Geophysical Research, v. 97, p. 10,997–11,009.

Allègre, C.J., Dupré, B., Lambert, B., and Richard, P., 1981, The subcontinental versus suboceanic debate. Lead-neodymium-strontium isotopes in primary basalts in a shield area: the Ahaggar volcanic suite: Earth and Planetary Science Letters, v. 52, p. 85–92, doi: 10.1016/0012-821X(81)90210-7.

Anderson, D.L., 2001, A statistical test of the two reservoir model for helium isotopes: Earth and Planetary Science Letters, v. 193, p. 77–82, doi: 10.1016/S0012-821X(01)00507-6.

Anderson, D.L., 2005, Scoring hotspots: The plume and plate paradigms, *in* Foulger, G.R., Natland, J.H., Presnall, D.C., and Anderson, D.L., eds., Plates, Plumes and Paradigms: Geological Society of America Special Paper 388, p. 31–54.

Anderson, D.L., and Natland, J.H., 2005, A brief history of the plume hypothesis and its competitors: Concepts and controversy, *in* Foulger, G.R., Natland, J.H., Presnall, D.C., and Anderson, D.L., eds., Plates, Plumes and Paradigms: Geological Society of America Special Paper 388, p. 119–145.

Ayadi, A., Dorbath, C., Lesquer, A., and Bezzeghoud, M., 2000, Crustal and upper mantle velocity structure of the Hoggar swell (central Sahara, Algeria): Physics of the Earth and Planetary Interiors, v. 118, p. 111–123, doi: 10.1016/S0031-9201(99)00134-X.

Azambre, B., and Girod, M., 1966, Phonolites agpaïtiques: Bulletin de la Société Française de Minéralogie et de Cristallographie, v. 90, p. 514–520.

Azzouni-Sekkal, A., Liégeois, J.P., Bechiri-Benmerzoug, F., Belaidi-Zinet, S., and Bonin, B., 2003, The "Taourirt" magmatic province, a marker of the closing stages of the Pan-African orogeny in the Tuareg shield: Review of the available data and Sr-Nd isotope evidence: Journal of African Earth Sciences, v. 37, p. 331–350, doi: 10.1016/j.jafrearsci.2003.07.001.

Benhallou, A.Z., 2000, Étude du volcanisme alcalin Cénozoïque de la région de Tahifet (Bloc d'Azrou N'fad, Hoggar central, Algérie) [Magister thesis]: Algiers, USTHB-FSTGAT, 164 p.

Bigi, G., Castellarin, R., Catalano, R., Coli, M., Cosentino, D., Dal Piaz, G.V., Lentini, F., Parotto, M., Patacca, E., Praturlon, A., Salvini, F., Sartori, R., Scandone, P., and Vai, G.B., 1989, Synthetic structural-kinematic map of Italy: Rome, Progetto Finilizzato Geodinamica, CNR, scale 1:2,000,000.

Black, R., and Girod, M., 1970, Late Paleozoic to recent igneous activity in West Africa and its relationship to basement structure, *in* Clifford, T.N., and Gass, I.G., eds., African Magmatism and Tectonics: Edinburgh, Oliver & Boyd, p. 185–210.

Black, R., Jaujou, M., and Pellaton, C., 1967, Notice explicative sur la carte géologique de l'Aïr, à l'échelle du 1/500,000: Direction des Mines et de la Géologie, République du Niger; Paris, Editions du BRGM, 57 p.

Black, R., Latouche, L., Liégeois, J.P., Caby, R., and Bertrand, J.M., 1994, Pan-African displaced terranes in the Tuareg shield (central Sahara): Geology, v. 22, p. 641–644, doi: 10.1130/0091-7613(1994)022<0641:PADTIT>2.3.CO;2.

Bonin, B., 2004, Do coeval mafic and felsic magmas in post-collisional to within-plate regimes necessarily imply two contrasting, mantle and crustal, sources? A review: Lithos, v. 78, p. 1–24, doi: 10.1016/j.lithos.2004.04.042.

Burke, K., 1996, The African plate: South African Journal of Geology, v. 99, p. 339–410.

Cheilletz, A., Bertrand, J.M.L., Charoy, B., Moulahoum, O., Bouabsa, L., Farrar, E., Zimmerman, J.L., Dautel, D., Archibald, D.A., and Boullier, A.M., 1992, Géochimie et géochronologie Rb-Sr, K-Ar et ^{40}Ar/^{39}Ar des complexes granitiques Panafricains de la région de Tamanrasset (Algérie): Relations avec les minéralisations Sn-W associées et l'évolution tectonique du Hoggar central: Bulletin de la Société Géologique de France, v. 163, p. 733–750.

Chéry, J., and Vernant, P., 2006, Lithospheric elasticity promotes episodic fault activity: Earth and Planetary Science Letters, v. 243, p. 211–217, doi: 10.1016/j.epsl.2005.12.014.

Conquéré, F., and Girod, M., 1968, Contribution à l'étude des paragenèses des basaltes alcalins: Les spinelles du volcan de l'Oued Temorte (Massif de l'Atakor, Sahara Algérien): Contributions to Mineralogy and Petrology, v. 20, p. 1–29, doi: 10.1007/BF00371063.

Courtillot, V., Davaille, A., Besse, J., and Stock, J., 2003, Three distinct types of hotspots in the Earth's mantle: Earth and Planetary Science Letters, v. 205, p. 295–308, doi: 10.1016/S0012-821X(02)01048-8.

Dautria, J.M., Liotard, J.M., Cabanes, N., Girod, M., and Briqueu, L., 1987, Amphibole-rich xenoliths and host alkali basalts: Petrogenetic constraints and implications on the recent evolution of the upper mantle beneath Ahaggar (central Sahara, southern Algeria): Contributions to Mineralogy and Petrology, v. 95, p. 133–144, doi: 10.1007/BF00381263.

Dautria, J.M., Dostal, J., Dupuy, C., and Liotard, J.M., 1988, Geochemistry and petrogenesis of alkali basalts from Tahalra (Hoggar, northwest Africa): Chemical Geology, v. 69, p. 17–35, doi: 10.1016/0009-2541(88)90155-6.

Duggan, M.B., 1990, Wilkinsonite, $Na_2Fe^{2+}_4Fe^{3+}_2Si_6O_{20}$, a new member of the aenigmatite group from the Warrumbungle volcano, New South Wales, Australia: American Mineralogist, v. 75, p. 694–701.

Dupuy, C., Chikhaoui, M., and Dostal, J., 1993, Trace element and isotopic geochemistry of Cenozoic alkali basaltic lavas from the Atakor (central Sahara): Geochemical Journal, v. 27, p. 131–145.

Eby, G.N., 1992, Chemical subdivision of the A-type granitoids: Petrogenetic and tectonic implications: Geology, v. 20, p. 641–644, doi: 10.1130/0091-7613(1992)020<0641:CSOTAT>2.3.CO;2.

Fabre, J., (2005). Géologie du Sahara occidental et central. Série/Reeks: Tervuren African Geosciences Collection, MRAC Tervuren, Belgique, 572 p.

Fitton, J.G., 1987. The Cameroon line, West Africa: A comparison between oceanic and continental alkaline volcanism, *in* Fitton, J.G., and Upton, B.G.J., eds., Alkaline Igneous Rocks: Geological Society of London Special Publication 30, p. 273–291.

Frizon de Lamotte, D., 2006, Some recent developments on the Maghreb geodynamics: Comptes Rendus Geoscience, v. 338, p. 1–10, doi: 10.1016/j.crte.2005.11.006.

Girod, M., 1971, Le massif volcanique de l'Atakor (Hoggar, Sahara Algérien). Étude pétrographique, structurale et volcanologique: Paris, Centre de Recherches sur les Zones Arides, série Géologie, no. 12, Éditions du Centre National de la Recherche Scientifique, 158 p.

Gradstein, F.M., Ogg, J.G., Smith, A.G., Bleeker, W., and Lourens, L.J., 2004, A new geologic time scale, with special reference to Precambrian and Neogene: Episodes, v. 27, p. 83–100.

Grandjean, A., 1962, Les séismes au Hoggar: Travaux de l'Institut des Recherches Sahariennes, v. 21, p. 187.

Hirschmann, M.M., Kogiso, T., Baker, M.B., and Stolper, E.M., 2003, Alkalic magmas generated by partial melting of garnet pyroxenite: Geology, v. 31, p. 481–484, doi: 10.1130/0091-7613(2003)031<0481:AMGBPM>2.0.CO;2.

Jolivet, L., and Faccenna, C., 2000, Mediterranean extension and the Africa-Eurasia collision: Tectonics, v. 19, p. 1095–1106, doi: 10.1029/2000TC900018.

Jolivet, L., Faccenna, C., D'Agostino, N., Fournier, M., and Worrall, D., 1999, The kinematics of back-arc basins, examples from the Tyrrhenian, Aegean and Japan Seas, *in* Mac Niocaill, C., and Ryan, P.D., eds., Continental Tectonics: Geological Society of London Special Publication 164, p. 21–53.

King, S.D., and Anderson, D.L., 1998, Edge-driven convection: Earth and Planetary Science Letters, v. 160, p. 289–296, doi: 10.1016/S0012-821X(98)00089-2.

Le Bas, M.J., Le Maitre, R.W., Streckeisen, A., and Zanettin, B., 1986, A chemical classification of volcanic rocks based on the total alkali–silica diagram: Journal of Petrology, v. 27, p. 745–750.

Le Bas, M.J., Le Maitre, R.W., and Woolley, A.R., 1992, The construction of the total alkali–silica chemical classification of volcanic rocks: Mineralogy and Petrology, v. 46, p. 1–22, doi: 10.1007/BF01160698.

Le Maitre, R.W., ed., 1989, A Classification of Igneous Rocks and Glossary of Terms: Recommendations of the International Union of Geosciences Subcommission on the Systematics of Igneous Rocks: Oxford, Blackwell Scientific Publications, 193 p.

Le Maitre, R.W., ed., 2002. Igneous Rocks: A Classification and Glossary of Terms (2nd edition): Recommendations of the International Union of

Geosciences Subcommission on the Systematics of Igneous Rocks: Cambridge, Cambridge University Press, 236 p.

Lesquer, A., Bourmatte, A., Ly, S., and Dautria, J.M., 1989, First heat flow determination from the central Sahara: Relationship with the Pan-African belt and Hoggar domal uplift: Journal of African Earth Sciences, v. 9, p. 41–48, doi: 10.1016/0899-5362(89)90006-7.

Liégeois, J.P., Benhallou, A., Azzouni-Sekkal, A., Yahiaoui, R., and Bonin, B., 2005. The Hoggar swell and volcanism: Reactivation of the Precambrian Tuareg shield during Alpine convergence and West African Cenozoic volcanism, *in* Foulger, G.R., Natland, J.H., Presnall, D.C., and Anderson, D.L., eds., Plates, Plumes and Paradigms: Geological Society of America Special Paper 388, p. 379–400.

Lustrino, M., 2000, Volcanic activity from the Neogene to the present evolution of the Western Mediterranean area: A review: Ofioliti, v. 25, p. 87–101.

Maury, R.C., Fourcade, S., Coulon, C., El Azzouzi, M'H., Bellon, H., Coutelle, A., Ouabadi, A., Semroud, B., Megartsi, M'H., Cotten, J., Belanteur, O., Louni-Hacini, A., Piqué, A., Capdevila, R., Hernandez, J., and Rehault, J.P., 2000, Post-collisional Neogene magmatism in the Mediterranean Maghreb margin: A consequence of slab-breakoff: Comptes Rendus de l'Académie des Sciences, Paris, v. 331, p. 159–173.

Maza, M., 1998, Transition magmatisme tholéïitique-alcalin en contexte intra-continental: Exemple du "point chaud" de l'Ahaggar. Les complexes volcano-plutoniques annulaires du Sud-Amadghor et le district de Serouenout (Ahaggar central, Algérie) [Thèse de doctorat en Sciences]: Montpellier, Université Montpellier II–Sciences et Techniques du Languedoc, 200 p.

Maza, M., Briqueu, L., Dautria, J.M., and Bosch, D., 1998, Le complexe annulaire d'âge Oligocène de l'Achkal (Hoggar central, sud Algérie): Témoin de la transition au Cénozoïque entre les magmatismes tholéitique et alcalin. Évidences par les isotopes du Sr, Nd et Pb: Comptes Rendus Geoscience, v. 327, p. 167–172.

McDonough, W.F., and Sun, S.-s., 1995, The composition of the Earth: Chemical Geology, v. 120, p. 223–235, doi: 10.1016/0009-2541(94)00140-4.

McDonough, W.F., Sun, S.-s., Ringwood, A.E., Jagoutz, E., and Hofmann, A.W., 1992, Potassium, rubidium, and cesium in the Earth and Moon and the evolution of the mantle of the Earth: Geochimica et Cosmochimica Acta, v. 56, p. 1001–1012, doi: 10.1016/0016-7037(92)90043-I.

Meibom, A., and Anderson, D.L., 2004, The statistical upper mantle assemblage: Earth and Planetary Science Letters, v. 217, p. 123–139, doi: 10.1016/S0012-821X(03)00573-9.

Niu, Y., and O'Hara, M.J., 2003, Origin of ocean island basalts: A new perspective from petrology, geochemistry, and mineral physics considerations: Journal of Geophysical Research, v. 108, p. 2209–2228, doi: 10.1029/2002JB002048.

Pearce, J.A., Harris, N.B.W., and Tindle, A.G., 1984, Trace element discrimination diagrams for the tectonic interpretation of granitic rocks: Journal of Petrology, v. 25, p. 956–983.

Pik, R., Marty, B., and Hilton, D.R., 2006, How many plumes in Africa? The geochemical point of view: Chemical Geology, v. 226, p. 100–114, doi: 10.1016/j.chemgeo.2005.09.016.

Rémy, J.M., 1967, Étude géologique et volcanologique du sud-est de l'Amadror en Ahaggar (Sahara central): Nancy, Sciences de la Terre, Mémoire 10, 192 p.

Ritsema, J., 2005, Global seismic structure maps, *in* Foulger, G.R., Natland, J.H., Presnall, D.C., and Anderson, D.L., eds., Plates, Plumes and Paradigms: Geological Society of America Special Paper 388, p. 11–18.

Rognon, P., 1967, Le massif de l'Atakor et ses bordures (Sahara central). Étude géomorphologique: Paris, Éditions du Centre National de la Recherche Scientifique, 555 p.

Rognon, P., Gourinard, Y., and Bandet, Y., 1981, Un épisode de climat aride dans l'Atakor (Hoggar) vers 1.5 Ma (datations K/Ar) et sa place dans le contexte paléoclimatique du Plio-Pléistocène Africain: Bulletin de la Société Géologique de France, v. XXIII (7° série), p. 313–318.

Rognon, P., Gourinard, Y., Bandet, Y., Koeniguer, J.C., and Delteil-Desneux, F., 1983, Précisions chronologiques sur l'évolution volcano-tectonique et géochronologique de l'Atakor (Hoggar): Apports des données radiométriques (K/Ar) et paléoclimatique du Plio-Pleistocène Africain: Bulletin de la Société Géologique de France, v. XXV (7° série), p. 973–980.

Rosenbaum, G., Lister, G.S., and Duboz, C., 2002, Reconstruction of the tectonic evolution of the Western Mediterranean since the Oligocene: Journal of the Virtual Explorer, v. 8, p. 105–124.

Saadi, M., 1982, Shéma structural du Maroc: Notes et Mémoires du Service Géologique du Maroc, v. 278B, attached color map, scale 1:4,000,000.

Savelli, C., 2002, Time-space distribution of magmatic activity in the Western Mediterranean and peripheral orogens during the past 30 Ma (a stimulus to geodynamic considerations): Journal of Geodynamics, v. 34, p. 99–126, doi: 10.1016/S0264-3707(02)00026-1.

Sebai, A., Stutzmann, E., Montagner, J.P., Sicilia, D., and Beucler, E., 2006, Anisotropic structure of the African upper mantle from Rayleigh and Love wave tomography: Physics of the Earth and Planetary Interiors, v. 155, p. 48–62, doi: 10.1016/j.pepi.2005.09.009.

Sébrier, M., Siame, L., Zouine, M., Winter, T., Leturmy, P., and Missenard, Y., 2006, Active tectonics in the Moroccan High Atlas: Comptes Rendus Geoscience, v. 338, p. 65–79, doi: 10.1016/j.crte.2005.12.001.

Shapiro, N.M., and Ritzwoller, M.H., 2002, Monte-Carlo inversion for a global shear velocity model of the crust and upper mantle: Geophysical Journal International, v. 151, p. 88–105, doi: 10.1046/j.1365-246X.2002.01742.x.

Sleep, N.H., 1990, Hot spots and mantle plumes: Some phenomenology: Journal of Geophysical Research, v. 95, p. 6715–6736.

Sun, S.-s., and McDonough, W.F., 1989, Chemical and isotopic systematics of oceanic basalts: Implications for mantle composition and processes, *in* Saunders, A.D., and Norry, M.J., eds., Magmatism in the Ocean Basins: Geological Society of London Special Publication 42, p. 313–345.

Vai, G.B., 2001, Structure and stratigraphy: An overview, *in* Vai, G.B., and Martini, I.P., eds., Anatomy of an Orogen: The Apennines and Adjacent Mediterranean Basins: Bodmin, Cornwall, Great Britain, Kluwer Academic Publishers, p. 15–32.

Weaver, B.L., 1991a, Trace element evidence for the origin of ocean-island basalts: Geology, v. 19, p. 123–126, doi: 10.1130/0091-7613 (1991)019<0123:TEEFTO>2.3.CO;2.

Weaver, B.L., 1991b, The origin of ocean island basalt end-member compositions: Trace element and isotopic constraints: Earth and Planetary Science Letters, v. 104, p. 381–397, doi: 10.1016/0012-821X(91)90217-6.

Wilson, M., and Downes, H., 1991, Tertiary–Quaternary extension-related alkaline magmatism in western and central Europe: Journal of Petrology, v. 32, p. 811–849.

Yahiaoui, R., 2003, Étude du volcanisme alcalin de la région de l'Assekrem (Hoggar central), étude pétrographique, minéralogique, géochimique et géobarométrique [Magister thesis]: Algiers, USTHB-FSTGAT, 164 p.